THE JOURNAL OF BIOLOGICAL CHEMISTRY VOL. 287, NO. 20, pp. 16073–16087, May 11, 2012

Structure-dependent Pseudoreceptor Intracellular Traffic of Adamantyl Globotriaosyl Ceramide Mimics*[S]

Received for publication, October 28, 2011, and in revised form, March 12, 2012 Published, JBC Papers in Press, March 14, 2012, DOI 10.1074/jbc.M111.318196

Mitsumasa Saito[‡1], Murugespillai Mylvaganum[‡], Patty Tam[§¶], Anton Novak[‡], Beth Binnington[‡], and Clifford Lingwood[‡§¶2]

From the [‡]Research Institute, Program in Molecular Structure and Function, Hospital for Sick Children, Toronto, Ontario M5G 1X8, Canada and the Departments of [§]Biochemistry and [¶]Laboratory Medicine and Pathobiology, University of Toronto, Toronto, Ontario M5S 1A1, Canada

Background: Verotoxin internalization and retrograde transport to the Golgi/ER is mediated by Gb_3 glycolipid.
Results: Amphipathic Gb_3 mimics can alter binding, trafficking, and cytotoxicity of verotoxins.
Conclusion: The lipid moiety of Gb_3 analogues determines the trafficking of verotoxins.
Significance: Synthetic glycolipid analogues can function as membrane receptors to internalize bound ligand and subvert endogenous GSL traffic.

The verotoxin (VT) (Shiga toxin) receptor globotriaosyl ceramide (Gb_3), mediates VT1/VT2 retrograde transport to the endoplasmic reticulum (ER) for cytosolic A subunit access to inhibit protein synthesis. Adamantyl Gb_3 is an amphipathic competitive inhibitor of VT1/VT2 Gb_3 binding. However, Gb_3-negative VT-resistant CHO/Jurkat cells incorporate adaGb$_3$ to become VT1/VT2-sensitive. CarboxyadaGb$_3$, urea-adaGb$_3$, and hydroxyethyl adaGb$_3$, preferentially bound by VT2, also mediate VT1/VT2 cytotoxicity. VT1/VT2 internalize to early endosomes but not to Golgi/ER. AdabisGb$_3$ (two deacyl Gb_3s linked to adamantane) protects against VT1/VT2 more effectively than adaGb$_3$ without incorporating into Gb_3-negative cells. AdaGb$_3$ (but not hydroxyethyl adaGb$_3$) incorporation into Gb_3-positive Vero cells rendered punctate cell surface VT1/VT2 binding uniform and subverted subsequent Gb_3-dependent retrograde transport to Golgi/ER to render cytotoxicity (reduced for VT1 but not VT2) brefeldin A-resistant. VT2-induced vacuolation was maintained in adaGb$_3$-treated Vero cells, but vacuolar membrane VT2 was lost. AdaGb$_3$ destabilized membrane cholesterol and reduced Gb_3 cholesterol stabilization in phospholipid liposomes. Cholera toxin GM1-mediated Golgi/ER targeting was unaffected by adaGb$_3$. We demonstrate the novel, lipid-dependent, pseudoreceptor function of Gb_3 mimics and their structure-dependent modulation of endogenous intracellular Gb_3 vesicular traffic.

Verotoxin (VT)[3] comprises a family of *Escherichia coli*-derived AB_5 subunit toxins (also termed Shiga toxins). Verotoxin cytopathology is targeted via the B subunit pentamer of the holotoxin binding to its receptor glycosphingolipid (GSL), globotriaosyl ceramide (Gb_3; also known as the p^k blood group antigen (1) and CD77, a human B cell marker (2)). VT1 and VT2 (60% identical at the nucleotide level (3)) are the primary verotoxins associated with clinical disease (4). Gastrointestinal infection with verotoxin-producing *E. coli* can result in the pathology of hemorrhagic colitis, which may precede the more severe hemolytic uremic syndrome (HUS), a renal pathology characterized by a triad of symptoms, thrombocytopenia, anemia, and renal glomerular microangiopathy (5). Hemorrhagic colitis is mediated via VT targeting Gb_3 within the submucosal microvasculature of the GI tract. Subsequent systemic verotoxemia results in toxin access to renal glomerular endothelial cells, which also express Gb_3 (6) to mediate endothelial cell damage, blood vessel occlusion, glomerular infarct, and subsequent hemolysis. HUS, primarily a disease of the very young and elderly (7), currently retains an approximately 5% mortality, and estimates of morbidity range as high as 30%. The recent German outbreak of enteroaggregative, VT2-expressing *E. coli* infections (8, 9) with an HUS incidence reaching 25% and a preponderance of female adult cases indicates major, unsuspected knowledge gaps in VT-induced pathology.

For reasons as yet unclear, VT2 is more frequently associated with clinical disease than VT1 (10, 11), despite the fact that VT1 is a more potent cytotoxin *in vitro* (12) and both toxins bind to

* This work was supported by Canadian Institutes of Health Research Grant MT 13747 and grants from Ontario HIV Treatment Network and Canfar.
[S] This article contains supplemental Tables 1 and 2 and Figs. 1–4.
[1] Present address: Dept. of Bacteriology, Faculty of Medical Sciences, Kyushu University, 3-1-1 Maidashi, Higashi-ku, Fukuoka 812-8582, Japan. Tel.: 81-92-642-6128; E-mail: msaito@bact.med.kyushu-u.ac.jp.
[2] To whom correspondence should be addressed: Clifford Lingwood Molecular Structure & Function Program, Research Institute, Hospital for Sick Children, 555 University Ave., Toronto, Ontario M5G 1X8, Canada. E-mail: cling@sickkids.on.ca.
[3] The abbreviations used are: VT, verotoxin; GSL, glycosphingolipid; Gb_3, globotriaosyl ceramide; adaGSL, adamantyl GSL; adaGb$_3$, adamantyl Gb_3, (2*S*,3*R*,4*E*)-2-(1-adamantane)-acetamido-3-hydroxyl-4-octadecenyl-(α-D-galactotopyranosyl)-(1–4)-(β-galactopyranosyl)-(1–4)-β-D-glucopyranoside; carboxyadaGb$_3$, (2*S*,3*R*,4*E*)-2-(1-(3-carboxymethyl)-adamantanacetamido)-3-hydroxyl-4-octadecenyl-(α-D-galactotopyranosyl)-(1–4)-(β-galactopyranosyl)-(1–4)-β-D-glucopyranoside; urea-adaGb$_3$, (2*S*,3*R*,4*E*)-2-(1-(3-(3-(1,3-diisopropyl)-ureido)-adamantanacetamido)-3-hydroxyl-4-octadecenyl-(α-D-galactotopyranosyl)-(1–4)-(β-galactopyranosyl)-(1–4)-β-D-glucopyranoside; OHEtadaGb$_3$, (2*S*,3*R*,4*E*)-2-(1-(3-(*N*-2-hydroxyethyl)-carbamoyl)-adamantanacetamido)-3-hydroxyl-4-octadecenyl-(α-D-galactotopyranosyl)-(1–4)-(β-galactopyranosyl)-(1–4)-β-D-glucopyranoside; adabisGb$_3$, adamantylbisGb$_3$; GM1, sialyl gangliotetraosyl ceramide; BFA, brefeldin A; ER, endoplasmic reticulum; NBD, 12-(*N*-methyl-*N*-(7-nitrobenz-2-oxa-1,3-diazol-4-yl)); HUS, hemolytic uremic syndrome; TGN, trans-Golgi network; SPM, sphingomyelin; MβCD, methyl-β-cyclodextrin; CT, cholera toxin; CTB, cholera toxin B subunit; VT1B, VT1 B-subunit; PC, phosphatidylcholine; CD50, dose required for 50% cell killing.

the same receptor (13). Despite a common receptor Gb$_3$, VT1 and VT2 preferentially bind different and shared epitopes within the Gb$_3$ carbohydrate (14, 15), which may be differentially available within different lipid contexts (12). Such differential receptor binding results in coincident but also discreet VT1 and VT2 binding sites on the surface of sensitive cells (12, 16) and within human renal tissue (15, 17). Cholesterol within human renal glomeruli can mask Gb$_3$ to prevent VT1 and VT2 binding (15, 17). Unlike VT1, VT2 can induce the formation of intracellular vacuoles in a subfraction of susceptible renal epithelial cells (12).

Cell membrane GSL carbohydrate presentation for ligand binding is complex, being a function of both the highly heterogeneous composition of the membrane-embedded ceramide and a lateral association with other membrane lipids, most notably cholesterol (18), to form domains of differential membrane order (19). Molecular simulation shows that the cholesterol-GSL interaction can alter the GSL carbohydrate conformation (18, 20) from a membrane-perpendicular to -parallel format. Cholesterol can mask GSLs to prevent appropriate ligand binding in tissues (15, 17, 20) and in model and cell membranes (20, 21). Nevertheless, to mediate cell cytotoxicity *in vitro*, Gb$_3$ must be expressed in what are termed cell surface lipid microdomains or rafts (22, 23), in which the concentration of GSLs and cholesterol and membrane order are significantly increased (24). The renal glomerulus is the target of the VT-induced pathology of HUS, and glomerular Gb$_3$ is within such domains (17). We propose that adaGSLs, unlike the parent GSL, will not interact with cholesterol; indeed, the adamantane frame may partially substitute for cholesterol to provide a mimic of the GSL-cholesterol complex (25).

Membrane Gb$_3$ within such domains mediates both clathrin-dependent (26) and -independent (27) VT internalization and subsequent "retrograde transport," from the cell surface through endosomes, trans-Golgi network (TGN), and Golgi to the ER (28), where the A subunit is translocated to the cytosol for inhibition of protein synthesis (29). When VT binds to non-raft Gb$_3$, internalization of the toxin receptor complex mediates the transport of the toxin to the lysosome for degradation, without the induction of cytotoxicity (22, 30). This may be similar to the abnormal transport of accumulated GSLs and cholesterol to lysosomes in GSL storage diseases (31). Cholesterol depletion (27) or modulation (32) can also prevent the GSL endosome-TGN transition. A balance of GSL-cholesterol interaction may be required for retrograde transport.

Verotoxin binding to the Gb$_3$ oligosaccharide is modulated by the lipid moiety of Gb$_3$ (33, 34) and the membrane environment in which Gb$_3$ is presented (35). This has been termed "aglycone modulation of GSL receptor function" (36). The requirement for retrograde transport of the toxin receptor complex to the endoplasmic reticulum is shared by the cholera toxin/GM1 receptor interaction (37, 38). Exogenous GSL analogues in which the native fatty acid is replaced by a fluorescent group (*e.g.* BODIPY or NBD) also demonstrate retrograde transport from the cell surface to the Golgi (39).

Several groups have developed receptor analogues based on the Gb$_3$ carbohydrate sequence coupled to polymeric or pentameric scaffolds (40–42) to develop specific receptor-based means to prevent the *in vivo* cytotoxicity, which may follow verotoxin-producing *E. coli* infection. The binding affinity of the VT B subunit pentamer for the lipid-free oligosaccharide is much reduced compared with native Gb$_3$ glycolipid (43), but this can be largely countered by multivalency (41), particularly when tailored to accommodate the pentameric geometry of the receptor B subunits displayed within the VT holotoxin (40, 42).

An additional approach is to try to utilize the inherent high affinity binding of the native Gb$_3$ glycolipid. Substitution of the Gb$_3$ fatty acid with an adamantane frame provided a water-soluble analog of Gb$_3$ that retained high affinity VT1 binding in an aqueous environment (44, 45). Although this analog proved an effective competitor to prevent VT1 and VT2 cytotoxicity *in vitro* (12), *in vivo*, the analog was found to augment rather than reduce VT2 cytopathology (46).

Our present studies indicate that this is due to a previously unrecognized property of such GSL analogues. We now show that adaGb$_3$ can partition into receptor-negative cells to render them VT1- and VT2-sensitive. This pseudoreceptor function is mediated via a novel intracellular routing pathway involving early endosomes. Moreover, we find that this adaGb$_3$ pathway can also hijack the endogenous cellular Gb$_3$-mediated retrograde transport of VT in sensitive cells to reroute traffic and induce resistance. This may relate to loss of interaction with cholesterol that we show for the adaGSL mimic. We have designed several new soluble adaGb$_3$ analogues and show this dominant rerouting of native intracellular GSL trafficking is prevented by chemical substitution within the adamantane frame, suggesting the existence of intramembrane vesicular trafficking cues.

A dimeric Gb$_3$ analog retains the VT1/VT2 inhibitory activity of adaGb$_3$ in solution but is unable to insert into cell membranes to show VT1/VT2 pseudoreceptor function. These studies demonstrate the importance of the lipid chemistry of Gb$_3$ in membrane incorporation and intracellular trafficking and illustrate a new approach against VT-induced cytopathology. Exogenous GSL mimics can be functionally trafficked in cells and, according to their lipid structure, subvert endogenous intracellular membrane GSL trafficking pathways.

EXPERIMENTAL PROCEDURES

Synthetic Compounds—Synthesis of the adamantyl analogues of Gb$_3$ (Fig. 1) is described in the supplemental material. Analogues were prepared for cell insertion as follows. Compounds were dried from solution in $CHCl_3$-CH_3OH (2:1, v/v) under N_2, resuspended in ethanol, sonicated briefly, dried under N_2, and resuspended in water at a concentration of 100 μM. To allow the analogues to reach an equilibrium state in solution, solutions were vortexed and sonicated for 30 s and then incubated at 37 °C for 2 h. Aliquots were dispensed into glass tubes, rapidly frozen on dry ice, and lyophilized overnight. The compounds were redissolved in chilled serum-free culture medium immediately before the addition to cells.

Reagents and Antibodies—Verotoxin 1 (VT1) and VT2 and VT1 B-subunit were purified as described previously (34, 46). Antibodies used were as follows. Mouse anti-VT1 mAb PH-1, reactive against the VT1 B-subunit and polyclonal rabbit anti-VT1 B-subunit, were prepared in our laboratory. Rabbit anti-

VT2 was a generous gift of Dr. Glen Armstrong (University of Calgary). Goat anti-EEA1 (Santa Cruz Biotechnology, Inc.), mouse anti-Lamp-2 (Developmental Studies Hybridoma Bank, clone H4B4), rabbit anti-Rab6 (Santa Cruz Biotechnology, Inc.), and rabbit anti-calnexin (Enzo Life Sciences) were obtained as indicated. Brefeldin A, cholera toxin B-subunit, sphingomyelin (SPM), methyl-β-cyclodextrin (MβCD), cholesterol, egg phosphatidylcholine (PC), and crystal violet were from Sigma. Fluorescence mounting medium was from Dako, and paraformaldehyde was from EM Sciences. [^{3}H]cholesterol and Cy3 were from GE Healthcare. Alexa Fluor 488 pentafluorophenyl ester, DiI LDL, DAPI, and Texas Red sulfonyl chloride were from Molecular Probes. Proteins were labeled with fluorophores using standard conditions as recommended by the manufacturer and isolated by gel filtration using G-25.

Cell Culture—Vero cells were grown in Eagle's minimum essential medium, 5% FCS, CHO; HEK-293 cells were grown in DMEM, 10% FCS; and Jurkat cells were grown in RPMI 1640, 10% FCS at 37 °C, 5% CO_2. All tissue culture media and buffers were obtained from Wisent Inc.

Insertion of GSL Analogues into Cells—Cells were washed twice with serum-free RPMI 1640 with 20 mM Hepes (H-RPMI) and chilled on ice. Cells were then incubated with freshly dissolved adaGb$_3$-solution for 1 h at 4 °C. Serum-containing medium was added for 37 °C incubations exceeding 1 h.

Cell Cytotoxicity Assays—Vero and CHO cells seeded in 96-well cell culture plates (3×10^4 cells/well) were grown at 37 °C overnight. Jurkat cells were centrifuged, washed twice with chilled H-RPMI, distributed in 96-well plates (5×10^4 cells/well), and chilled on ice.

Dilutions of adamantyl analogues were added to the cells and incubated on ice for 1 h. 10-fold serial VT1/VT2 or ricin dilutions were then added to the cells and incubated at 37 °C. After 4 h, serum was added to a final concentration of 5%, and cells were incubated at 37 °C for another 68 h. In some experiments, 0.5 μg/ml brefeldin A (BFA) was added for 30 min at 37 °C before the addition of VT and maintained throughout. Due to the long term toxicity of BFA, cytotoxicity was measured after 18 h of toxin treatment.

At the end of the incubation period, live cells were fixed onto the wells using 2% formalin in PBS and stained with crystal violet as described (47). Dye was solubilized with 100 μl of 10% acetic acid, and optical density was read at 560 nm using an ELISA plate reader. Cell viability was expressed as a percentage of control cells, which were treated with neither VT nor adaGb3 analogues.

The ability of the adamantyl Gb$_3$ analogues in solution to block VT cytotoxicity to Gb$_3$+ve cells was assessed by prebinding the toxin and analogues prior to the addition to Vero cells. Dilutions (50 ng/ml to 0.03 pg/ml) of VT1 or VT2 in Eagle's minimum essential medium were prepared and mixed with an equal volume of adaGb$_3$ or adabisGb$_3$ (100, 50, 25, 12.5, 6.3, and 3.1 μM). After incubation at 37 °C for 60 min, 50 μl of the mixture was added to Vero cells in 96-well plates and incubated for 1 h at 37 °C. Cells were washed with Eagle's minimum essential medium and then incubated in complete medium for 72 h at 37 °C. Cell viability was measured as described above by crystal violet staining.

Confocal Fluorescence Microscopy—CHO and Jurkat cells were grown to 80% confluence on 12-mm gelatin-treated glass coverslips. Cells were washed twice with H-RPMI, chilled on ice, and then incubated with 50 μM adabisGb$_3$ or 20 μM adaGb$_3$ (CHO) or 10 μM adaGb$_3$ (Jurkat) in H-RPMI for 1 h on ice. For labeling of the cells with VT, 4 μg/ml Alexa Fluor 488-VT1 or Texas Red-VT2 was bound on ice for 1 h. Cells were washed with cold PBS and fixed with 4% paraformaldehyde in PBS. To observe the intracellular trafficking of VT, bound VT was internalized at 37 °C for 10 min, 1 h, or 6 h. At the end of the incubation period, the cells were fixed with 4% paraformaldehyde in PBS, permeabilized for 15 min at ambient temperature with 0.2% Triton X-100, and then blocked with 2% BSA. Verotoxins were detected with VT1- or VT2-specific antibodies and the organelle-specific antibodies to EEA1 (early endosomes), Rab6 (Golgi), Lamp-2 (late endosome/lysosome), or calnexin (ER), followed after washing with Alexa Fluor 488 or 546 anti-goat or 594 anti-rabbit secondary antibody.

Microscope Image Acquisition—Fluorescently stained cells were viewed with a Leica DMRE2 confocal microscope under oil at ×63 with a numerical aperture of 1.4 at ambient temperature. Fluorophores used were DAPI for nuclear staining, Alexa488 (for VT), Cy3 (for cholera toxin (CT)), Texas Red (for VT2), and Alexa 594 (secondary antibody). Images were captured with a Hamamatsu EM-CCD C9100 digital camera using Volocity 5.5.0. Confocal stacks were deconvolved with Volocity software by iterative restoration using calculated point spread functions. Composite images were assembled using Photoshop CS4 and Zeiss Image Examiner.

Isolation of Total Lipids from Cells and Detection by TLC—CHO cells (1×10^7 cells) and Jurkat cells (2.4×10^6 cells) were treated with 20 μM adaGb$_3$ or 50 μM adabisGb$_3$ for 1 h on ice and then washed with PBS. Cell suspensions in water were transferred into chloroform/methanol (2:1, v/v) and shaken vigorously overnight. After filtering the cell debris, the solvents were dried down, resuspended in methanolic NaOH for saponification, and then neutralized with NH_4HOAc and HCl. The samples were desalted using Sep-Pak C_{18} cartridges (Waters, Milford, MA). The lipids were eluted with methanol and chloroform/methanol (2:1), dried down, and redissolved in 100 μl of chloroform/methanol (2:1). The samples (10 μl each) were separated on two identical TLC plates (chloroform/methanol/water; 65:25:4), one for detection with orcinol and one for VT binding.

VT1 and VT2 Binding to Gb$_3$ and Analogues by TLC Overlay—After GSL separation, the TLC plates were dried and incubated with 1% fish gelatin in TBS for 3 h at room temperature and washed twice with TBS. The plates were incubated with VT1 B-subunit (0.35 μg/ml) or VT2 (2.5 μg/ml) overnight at 4 °C, with polyclonal rabbit anti-VT1 B-subunit (VT1B) or anti-VT2 for 3 h at room temperature, and with HRP-conjugated goat anti-rabbit IgG for 1 h at room temperature. Bound toxin was detected by development using 0.6 mg/ml 4-chloro-1-naphthol, 0.015% H_2O_2 in TBS.

Liposomal Assay of Glycosphingolipid-Cholesterol Interaction—The ability of Gb$_3$ as compared with adaGb$_3$ to interact with cholesterol in membranes was quantitated in liposomes by measuring the induced resistance to cholesterol extraction by MβCD, based on previous studies (48, 49). Multilamellar PC,

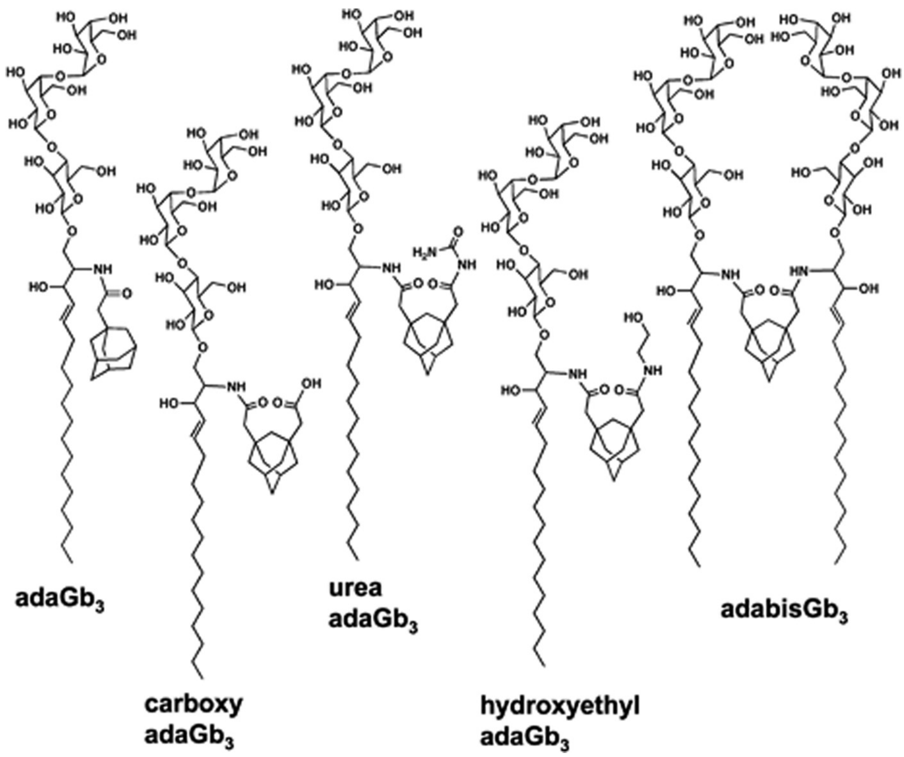

FIGURE 1. **Scheme for adaGb$_3$, carboxyadaGb$_3$, urea-adaGb$_3$, OHEtadaGb$_3$, and adabisGb$_3$.**

[^{3}H]cholesterol liposomes with or without Gb$_3$, SPM, or adaGb$_3$ were prepared. (*a*) 0.2 μmol of PC + 0.07 μmol of cholesterol (500,000 dpm), (*b*) 0.14 μmol of PC + 0.07 μmol of cholesterol + 0.07 μmol of Gb$_3$, and (*c*) 0.07 μmol of PC + 0.07 μmol of cholesterol + 0.07 μmol of Gb$_3$ or SPM + 0.07 μmol of adaGb$_3$ were dried together from organic solvent under N_2, freeze-dried, and vortexed in PBS for 30 min at room temperature to give a total lipid concentration of 500 μM in a total volume of 500 μl. Liposomes were briefly sonicated and incubated at 85 °C for 30 min with vortexing every 5 min, cooled to room temperature, centrifuged at 11,000 $\times$ *g* for 10 min, and washed in PBS. 50-μl aliquots were mixed with 50 μl of PBS with or without 0.5 mM MβCD at room temperature for 60 min with frequent vortexing. The suspension was centrifuged at 11,000 $\times$ *g* for 10 min, and tritium in the supernatant was counted in a scintillation counter.

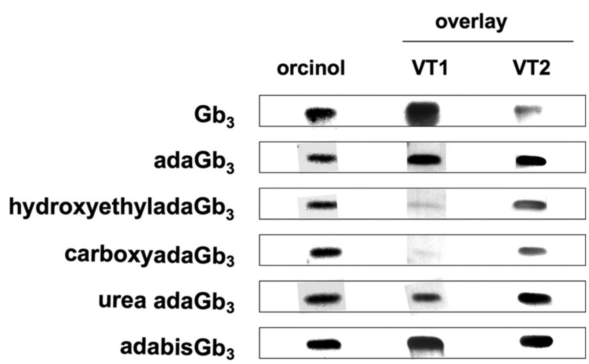

FIGURE 2. **VT1 and VT2 binding to Gb$_3$ and adaGb$_3$ analogues by TLC overlay.** The glycolipids (1.3 μg each) were separated by TLC and detected by orcinol or by binding of either VT1 or VT2. The binding to adaGb$_3$, OHEtadaGb$_3$, carboxyadaGb$_3$, urea-adaGb$_3$, and adabisGb$_3$ relative to Gb$_3$ was calculated from the band intensities: VT1, 80, 20, 6, 35, and 68%; VT2, 400, 275, 140, 310, and 315%.

RESULTS

Adamantyl Gb$_3$ Analogues—Five soluble adamantyl Gb$_3$ analogues were synthesized from deacyl(lyso)-Gb$_3$ (see supplemental material). The structures of these species are shown in Fig. 1. Different substitutions at the 2-position of the adamantane frame generated an acidic carboxyadaGb$_3$, a basic urea-adaGb$_3$, and a neutral hydroxyethyl adaGb$_3$ (OHEtadaGb$_3$). Coupling a second lyso-Gb$_3$ to carboxyadaGb$_3$ generated the dimeric adamantylbisGb$_3$ (adabisGb$_3$).

VT1/VT2 Binding to Synthetic Gb$_3$ Analogues—The VT binding activities of Gb$_3$, adaGb$_3$, OHEtadaGb$_3$, carboxyadaGb$_3$, urea-adaGb$_3$, and adabisGb$_3$ were compared by TLC overlay (Fig. 2). Gb$_3$ and each adaGb$_3$ analog were bound by VT1 and VT2. VT2/Gb$_3$ binding was weaker than that of VT1, as shown previously (46). However, VT2 bound all adaGb$_3$ species in preference to native Gb$_3$. AdaGb$_3$ and adabisGb$_3$ bound strongly to both VT1 and VT2.

AdaGb$_3$ Induction of VT1/VT2 Cytotoxicity to Gb$_3$-negative Cells—To assess the potential pseudoreceptor function of these adaGb$_3$ analogues, the Gb$_3$-negative, VT-resistant Jurkat and CHO cell lines were selected as potential targets for receptor "reconstitution."

Cells were incubated in the presence of adaGb$_3$ and then treated with VT1 or VT2. The resulting cytotoxicity curves (Fig. 3*A*) show that untreated CHO cells were resistant to VT1 and VT2 below 10 μg/ml and that Jurkat cells were resistant at <1 μg/ml, whereas 10–20% cells were killed at 10 μg/ml. Cells treated with adaGb$_3$, carboxyadaGb$_3$, OHEtadaGb$_3$, or urea-adaGb$_3$ all showed increased susceptibility to VT1 and VT2 cytotoxicity. Significantly greater VT sensitivity was induced in

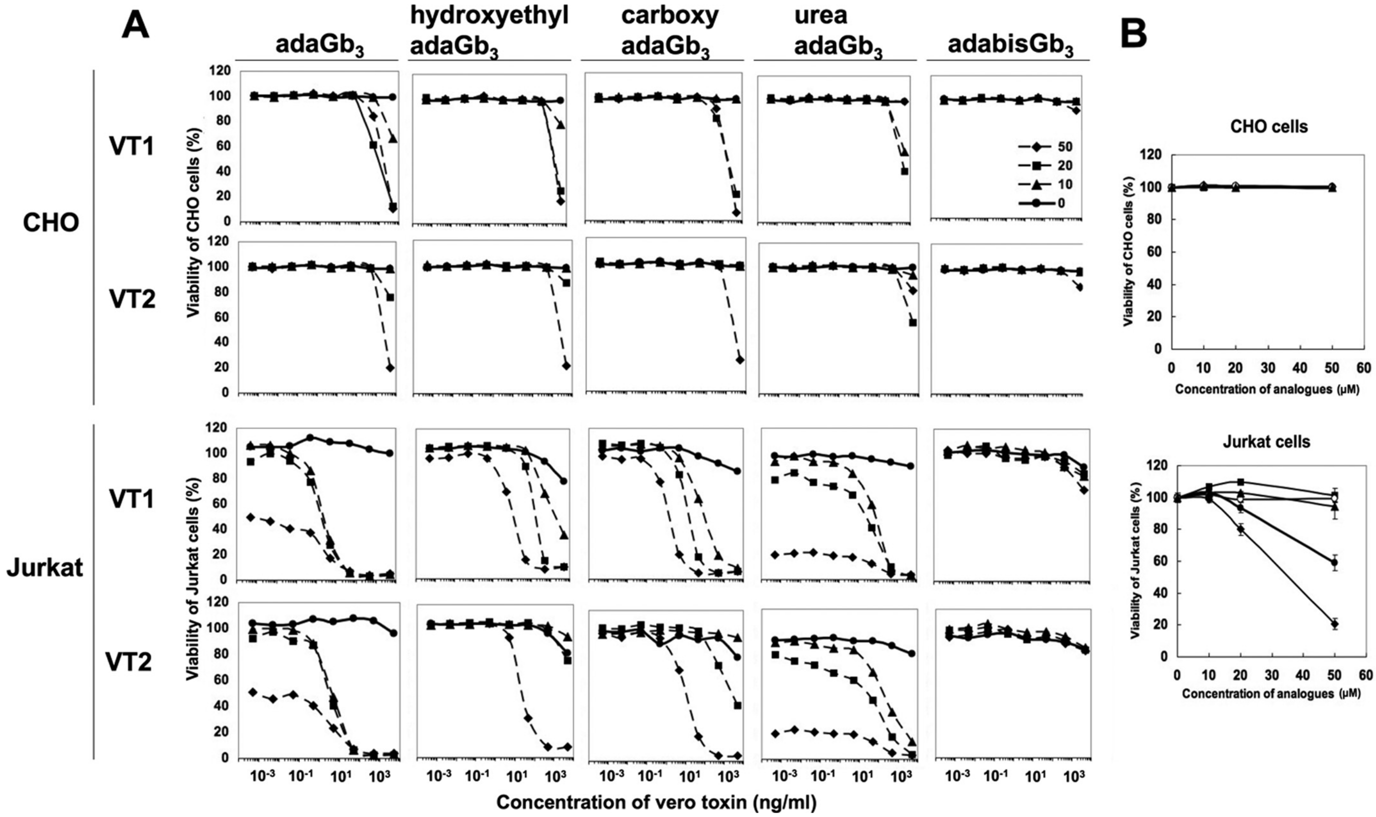

FIGURE 3. *A*, induction of VT1/VT2 toxicity in adaGb$_3$ analog-treated CHO and Jurkat cells. CHO or Jurkat cells were incubated with 0, 10, 20, or 50 μM adaGb$_3$ at 4 °C for 1 h. Cells were treated with 10-fold serial diluted VT1 or VT2 and incubated at 37 °C. Cell viability was monitored after 72 h and expressed as a percentage of control cells, which were treated with neither VT nor adaGb$_3$ analogues. *B*, effect of adaGb$_3$ analogues on CHO/Jurkat cell viability. CHO or Jurkat cells were incubated with 0, 10, 20, or 50 μM adaGb$_3$ (*closed circles*), OHEtadaGb$_3$ (*triangles*), carboxyadaGb$_3$ (*squares*), urea-adaGb$_3$ (*diamonds*), or adabisGb$_3$ (*open circles*) at 37 °C. Cell viability was monitored after 72 h and expressed as a percentage of non-treated control cells.

Jurkat, as compared with CHO cells. Indeed, reconstituted CHO cells were only sensitive to the highest dose of VT1 and VT2 tested and essentially only at the highest concentration of adaGb$_3$ analog added. The receptor-incorporated CHO cells were in general slightly more sensitive to VT1 than VT2. However, Jurkat cell VT1 and VT2 sensitivity was significantly increased following treatment with any of the adaGb$_3$ analogues. Again susceptibility to VT2 was slightly less than that of VT1, and the different adaGb$_3$ analogues showed varying degrees of induction of VT1 and VT2 sensitivity. Cells in which adaGb$_3$ was incorporated showed the greatest response to VT1 and VT2, with a CD_{50} of between 0.1 and 10 ng/ml according to adaGb$_3$ dosage. CarboxyadaGb$_3$-treated cells and OHEtadaGb$_3$-treated cells showed less VT1/VT2 sensitivity, with CD_{50} ranging from 1 to 100 ng/ml for VT1 and from 50 to 10,000 ng/ml for VT2 according to adaGb$_3$ analog dosage. Cells treated with urea-adaGb$_3$ were yet less sensitive to VT1 and VT2.

In contrast to the other adaGb$_3$ derivatives, treatment of Jurkat or CHO cells with adabisGb$_3$ had no subsequent effect on VT1 or VT2 sensitivity. AdabisGb3 treated cells remained resistant to VT1/VT2.

At high dosage, some adaGb$_3$ analogues were toxic to Jurkat cells (Fig. 3*B*). A concentration of $>$20 μM adaGb$_3$ or urea-adaGb$_3$ was toxic, whereas OHEtadaGb$_3$, carboxyadaGb$_3$, and adabisGb$_3$ were non-toxic at all doses. No analog showed cytotoxicity to CHO cells.

VT1/VT2 Binding to Gb$_3$ Analog-treated CHO/Jurkat Cells—AdaGb$_3$-treated CHO or Jurkat cells showed significant cell surface binding of fluorescent VT1 or VT2 at 4 °C (Fig. 4*A*). Cell membrane labeling was punctate, particularly for CHO cells. No VT binding to adabisGb$_3$-treated CHO or Jurkat cells was detected.

Cellular Uptake of AdaGb$_3$ or AdabisGb$_3$—To determine whether adabisGb$_3$ is incorporated into the target cell membrane but becomes receptor-inactive, we extracted total lipids from adaGb$_3$ or adabisGb$_3$-treated CHO (Fig. 4*B*) and Jurkat cells (Fig. 4*C*) and detected the analogues by VT1 binding in a TLC overlay assay. AdaGb$_3$ was incorporated into both Jurkat and CHO cells, whereas adabisGb$_3$ was not detected in the extracts of adabisGb$_3$-treated cells. These results show adaGb$_3$ inserted into the cell membrane of Gb$_3$-negative cells to provide a pseudoreceptor for VT1 and VT2. In contrast, adabisGb$_3$ does not incorporate into the cell membrane of Gb$_3$-negative cells.

Intracellular VT1 Trafficking in AdaGb$_3$- or OHEtadaGb$_3$-reconstituted Cells—Confocal microscopy was used to compare the intracellular trafficking of fluorescent VT1 bound to endogenous Gb$_3$ in Vero cells and adaGb$_3$ inserted into CHO or Jurkat cells. After 10 min at 37 °C, a large fraction of internalized VT1 colocalized with the early endosome marker EEA1 in both Vero cells and adaGb$_3$-treated CHO/Jurkat cells (Fig. 4*D*). The VT1 also colocalized with transferrin in the "reconstituted" cells at this time (not shown). After 1 h at 37 °C in Vero cells,

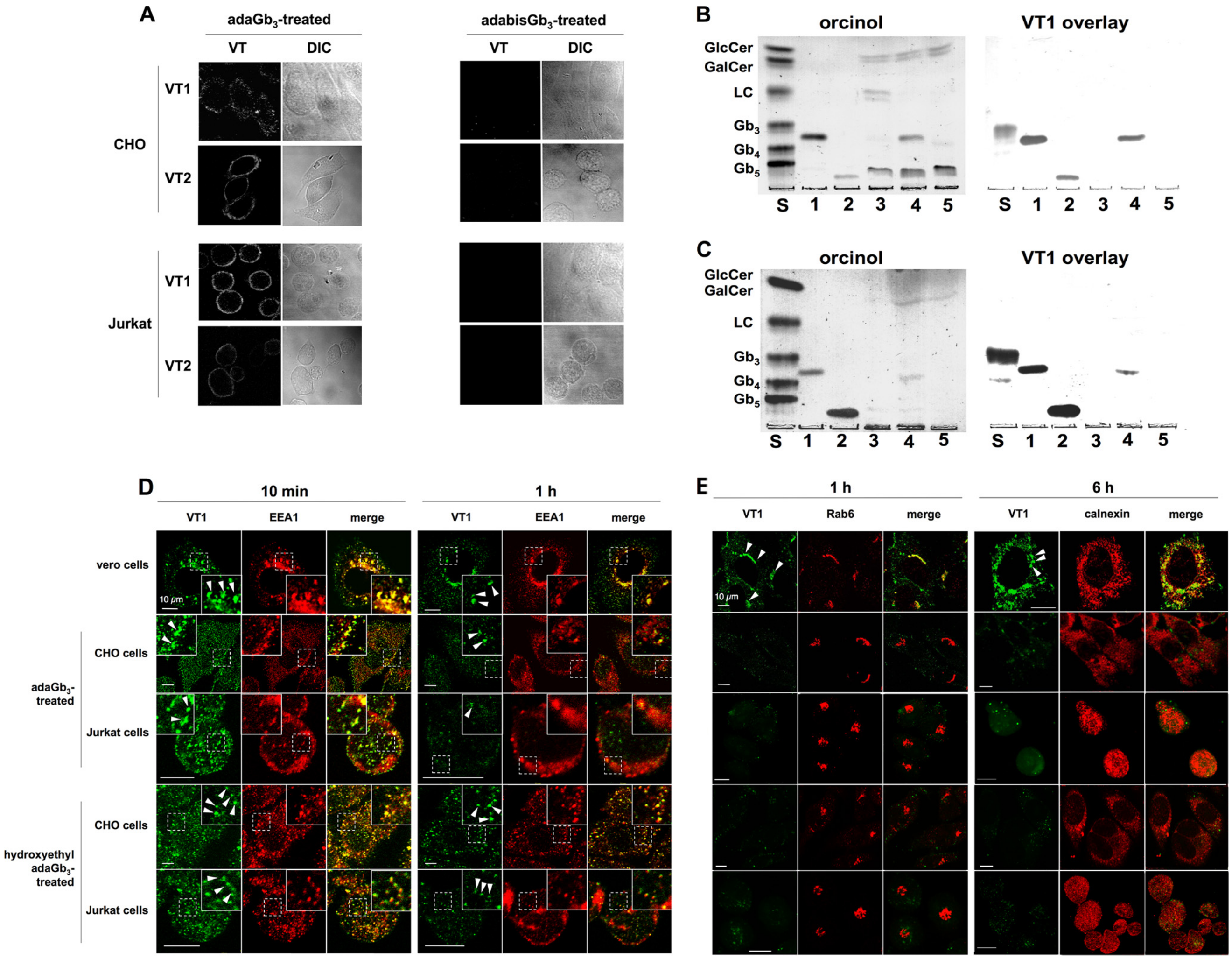

FIGURE 4. *A*, binding of VT1 or VT2 to adaGb$_3$- or adabisGb$_3$-treated Gb$_3$-negative cells. CHO cells were treated with 20 μM adaGb$_3$ (*left*) or 50 μM adabisGb$_3$ (*right*), and Jurkat cells were treated with 10 μM adaGb$_3$ (*left*) or 50 μM adabisGb$_3$ (*right*). Then 4 μg/ml Alexa488-VT1B or Texas Red-VT2 was added at 4 °C. After 1 h, cells were washed and fixed. Stained cells were viewed by confocal microscopy. *B* and *C*, TLC of total lipids from adaGb$_3$ or adabisGb$_3$-treated cells. Glycolipids were isolated from CHO and Jurkat cells, separated by TLC, and visualized with orcinol (*left*). VT binding to the lipids was detected by TLC overlay with VT1 B-subunit (*right*). *B*, *lane 1*, adaGb$_3$; *lane 2*, adabisGb$_3$; *lane 3*, total lipids of untreated CHO cells; *lane 4*, total lipids of adaGb$_3$-treated CHO cells; *lane 5*, total lipids of adabisGb$_3$-treated CHO cells. *C*, *lane 1*, adaGb$_3$; *lane 2*, adabisGb$_3$; *lane 3*, total lipids of untreated Jurkat cells; *lane 4*, total lipids of adaGb$_3$-treated Jurkat cells; *lane 5*, total lipids of adabisGb$_3$-treated Jurkat cells. *S*, standard glycolipid mixture (from the *top*, glucosylceramide, galactosylceramide, lactosylceramide, Gb$_3$, Gb$_4$, and Gb$_5$). *D* and *E*, trafficking of VT1 to the early endosome, Golgi, and ER in Vero cells compared with adaGb$_3$-treated or OHEtadaGb$_3$-treated CHO/Jurkat cells. VT1 was internalized at 37 °C for 10 min (*D*), 1 h (*D* and *E*), or 6 h (*E*) as indicated. After fixation and permeabilization, VT1 was detected with mAb PH-1/Alexa488 anti-mouse IgG (for EEA1 colocalization) or polyclonal anti-VT1B/Alexa488 anti-rabbit IgG (for RAb6 and calnexin colocalization). The early endosome marker EEA1 (*D*), Golgi marker Rab6 (*E*), or ER marker calnexin (*E*) was detected with Alexa546-labeled anti-goat or Alexa594 anti-rabbit antibodies (*red*). Fluorescently stained cells were viewed with a confocal microscope. Toxin colocalization (*arrowheads*) with organelle markers was quantitated (supplemental Table 1).

some of the internalized VT1 overlaps with the Golgi marker, Rab6 (Fig. 4*E*, *arrowheads*), and some remained colocalized with EEA1 (Fig. 4*D*). In adaGb$_3$- or OHEtadaGb$_3$-treated CHO/Jurkat cells, Rab6 coincidence with internalized VT1 was insignificant compared with Vero cells (Fig. 4*E*), although VT1 staining was much less overall. VT1 did not colocalize with the lysosomal marker, Lamp-2, at any time (supplemental Fig. 1). After 6 h, most VT1 colocalized with the ER marker calnexin in Vero cells (Fig. 4*E*). In contrast, most of VT1 was lost and rarely overlapped with calnexin in adaGb$_3$- or OHEtadaGb$_{33}$-treated CHO/Jurkat cells (Fig. 4*E*). Essentially the same results were found for OHEtadaGb$_3$-treated CHO and Jurkat cells (Fig. 4, *D* and *E*) (and for cells treated with carboxyl or urea-adaGb$_3$. Cells treated with adaSGC (sulfatide) did not bind VT (supplemental Fig. 2). Thus, these Gb$_3$ analogues mediate VT1 internalization to early endosomes, but trafficking to Golgi/ER, as seen in Gb$_3$-expressing, VT1/VT2-sensitive Vero cells, is not detectable. The differential targeting (quantitated in supplemental Table 1) provides an explanation for the reduced efficacy of adaGb$_3$, compared with natural Gb$_3$, to mediate VT cytotoxicity.

AdaGb$_3$ Treatment of VT-sensitive Vero Cells Subverts Endogenous Gb$_3$-mediated VT1 and VT2 Retrograde Transport—To assess any relationship between these "exogenous" *versus* "endogenous" trafficking pathways, Gb$_3$-expressing Vero cells were also "reconstituted" with adaGb$_3$ or OHEtadaGb$_3$. Cells were treated with VT1 or VT2, and cell viability was monitored after 72 h (Fig. 5*A*). Vero cell VT1 sensitivity was reduced 10-fold after adaGb$_3$ treatment, but little effect on VT2 sensitivity was seen.

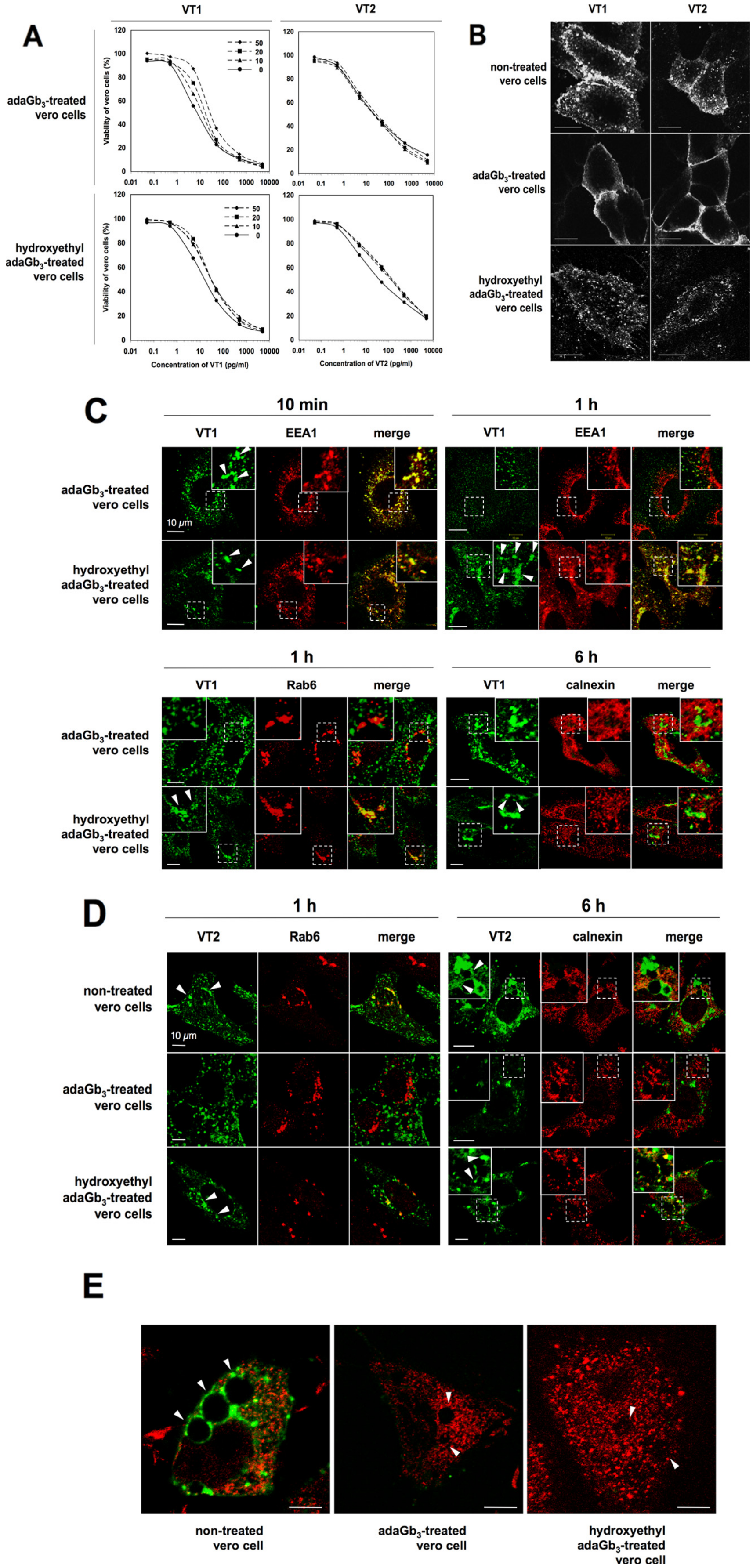
A
VT1
VT2
adaGb3-treated vero cells
hydroxyethyl adaGb3-treated vero cells
Viability of vero cells (%)
50
20
10
0
Concentration of VT1 (pg/ml)
Concentration of VT2 (pg/ml)
B
non-treated vero cells
C
10 min
1 h
6 h
EEA1
merge
Rab6
calnexin
10 μm
D
E
non-treated vero cell
adaGb3-treated vero cell
hydroxyethyl adaGb3-treated vero cell

OHEtadaGb$_3$ treatment of Vero cells had significantly less effect on VT1 sensitivity (Fig. 5*A*).

AdaGb$_3$ treatment of Vero cells altered the VT1 and VT2 cell surface staining pattern (Fig. 5*B*). Gb$_3$-expressing VT-sensitive Vero cells showed punctate cell surface binding, as observed previously (12). However, Vero cells treated with adaGb$_3$ showed a more uniform cell surface VT1/VT2 labeling pattern, as if adaGb$_3$ had served to fuse previously separate cell surface Gb$_3$ domains. In contrast, OHEtadaGb$_3$-treated Vero cells retained the punctate cell surface binding of non-treated Vero cells (Fig. 5*B*). Quantitation of cell surface binding showed that adaGb$_3$ treatment reduced the amount of Alexa488-VT1B bound by 20–30% (supplemental Fig. 3), consistent with loss of a GSL clustering component in membrane binding affinity (50).

The intracellular trafficking of VT1 in non-treated (Fig. 4, *D* and *E*) and in adaGb$_3$- or OHEtadaGb$_3$-treated Vero cells (Fig. 5*C*) was then compared. After 10 min at 37 °C, a large portion of internalized VT1 colocalized with early endosomal EEA1 in all cases. In non-treated Vero cells after 1 h at 37 °C, some internalized VT1 colocalized with the Golgi marker, Rab6 (Fig. 4*E*, *arrowheads*), and some remained with EEA1 (Fig. 4*D*). However, in adaGb$_3$-treated Vero cells after 1 h at 37 °C, little VT1 colocalized with EEA1, and VT1 coincidence with Rab6 (Fig. 5*C*) was far less than in non-treated Vero cells. In contrast, in OHEtadaGb$_3$-treated Vero cells, a large portion of internalized VT1 remained colocalized with EEA1 at 1 h (Fig. 5*C*) as in non-treated Vero cells. After 6 h, most VT1 colocalized with the ER marker calnexin in non-treated Vero cells (Fig. 4*E*). However, VT1 rarely overlapped with calnexin in adaGb$_3$-treated cells. In contrast, VT1/calnexin overlap at 6 h was retained in OHEtadaGb$_3$-treated Vero cells (Fig. 5*C*) although reduced compared with in non-treated Vero cells.

Because adaGb$_3$ was less effective to reduce VT2, as compared with VT1, Vero cell sensitivity (Fig. 5*A*), the intracellular trafficking of VT2 was compared in Vero and adaGb$_3$-treated Vero cells (Fig. 5*D*). After 1 h at 37 °C, some internalized VT2 was overlapping with the Golgi marker Rab6, in non-treated Vero cells (Fig. 5*C*, *arrowheads*). In adaGb$_3$-treated Vero cells, Rab6 coincidence with VT2 was barely detectable at 1 h, but in OHEtadaGb$_3$-treated Vero cells, internalized VT2 colocalized with Rab6 as for non-treated Vero cells. After 6 h of culture, significant VT2 colocalization with the ER marker calnexin in non-treated Vero cells was found. In contrast, VT2 showed no overlap with calnexin in adaGb$_3$-treated Vero cells at this time. However, for OHEtadaGb$_3$-treated cells, VT2/calnexin overlap (Fig. 5*C*) was similar to that in non-treated Vero cells after 6 h.

Thus, adaGb$_3$ changed the intracellular VT1 and VT2 trafficking in Gb$_3$-expressing cells. Initial endosomal entry was retained, but subsequent Golgi/ER traffic was compromised. OHEtadaGb$_3$ treatment had little obvious effect.

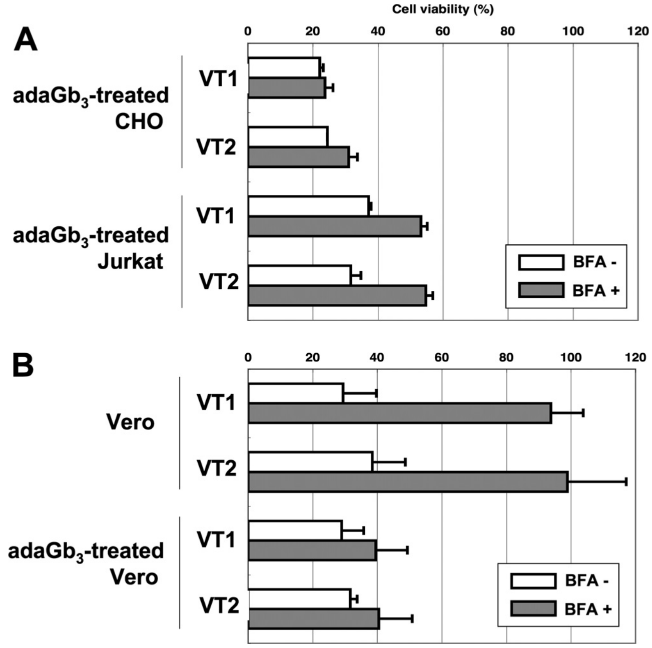

FIGURE 6. **Effect of BFA on VT1- and VT2-induced cell killing.** Cells were incubated ± 0.5 μg/ml BFA for 30 min prior to the VT addition. VT1 was added at 10 μg/ml for adaGb$_3$-treated CHO/Jurkat cells (*A*), 0.1 ng/ml for non-treated Vero cells (*B*, *top*), and 100 ng/ml for adaGb$_3$-treated Vero cells (*B*, *bottom*). VT2 was added at 10 μg/ml for adaGb$_3$-treated CHO/Jurkat cells, 1 ng/ml for non-treated Vero cells, and 100 ng/ml for adaGb$_3$-treated Vero cells. Cell viability was monitored after 21.5 h and expressed as a percentage of control cells in the absence of VT.

As previously reported (12), intracellular perinuclear vacuoles were detected in some VT2-treated Vero cells (Fig. 5*E*, *arrowheads*). VT2 vacuolation was retained for adaGb$_3$- or OHEtadaGb$_3$-treated Vero cells, but VT2 staining of these vesicles was lost (Fig. 5, *D* and *E*).

BFA, which prevents Golgi-dependent retrograde traffic, protects cells from VT1 (51). To confirm that intracellular VT trafficking in adaGb$_3$-treated cells mediates toxicity without Golgi access, the effects of BFA on VT-induced cytotoxicity in adaGb$_3$-treated CHO/Jurkat cells (Fig. 6*A*) and Vero cells (Fig. 6*B*) were compared. BFA was virtually ineffective to prevent VT1/VT2 killing of adaGb$_3$-treated CHO cells and provided minimal protection to adaGb$_3$-treated Jurkat cells (Fig. 6*A*). In contrast, BFA completely protected Vero cells against VT1/VT2 (Fig. 6*B*). However, for adaGb$_3$-treated Vero cells, VT1/VT2 cytotoxicity became BFA-resistant. These data indicate that intracellular VT traffic and toxicity in adaGb$_3$-treated CHO, Jurkat, and Vero cells is Golgi-independent.

FIGURE 5. *A*, toxicity of VT1/VT2 to adaGb$_3$- or OHEtadaGb$_3$-treated Vero cells. Vero cells were incubated with 0, 10, 20, or 50 μM adaGb$_3$ or OHEtadaGb$_3$ at 4 °C for 1 h. Cells were treated with 10-fold serially diluted VT1 or VT2 and incubated at 37 °C. Cell viability was monitored after 72 h and expressed as a percentage of control cells, which were treated with neither VT nor adaGb$_3$ analogues. *B*, staining of non-treated, adaGb$_3$-treated, or OHEtadaGb$_3$-treated Vero cells with fluorescent VT1 or VT2. Vero cells were treated with or without adaGb$_3$ or OHEtadaGb$_3$. Then Alexa488-VT1B or Texas Red-VT2 was bound on ice for 1 h. Cells were washed, fixed, and viewed with a confocal microscope. *Bar*, 10 μm. *C*, trafficking of VT1 in adaGb$_3$ or OHEtadaGb$_3$-treated Vero cells. VT1 was internalized at 37 °C for 10 min, 1 h, or 6 h in adaGb$_3$- or hydroxyethyl adaGb$_3$-treated Vero cells. VT1, EEA1, Rab6, and calnexin were localized as described in the legend to Fig. 4. *D*, trafficking of VT2 to the Golgi and ER in non-treated, adaGb$_3$-treated, or hydroxyethyl adaGb$_3$-treated Vero cells. Bound VT2 was internalized at 37 °C for 1 or 6 h. Cells were fixed, permeabilized, and labeled with anti-Rab6 (Golgi) or anti-calnexin (ER). Fluorescently stained cells were viewed with a confocal microscope. (Texas Red-VT2 is *pseudocolored green*, and organelle markers detected with anti-rabbit-Alexa488 *colored red*, for ease of comparison). *E*, VT2-induced vacuolation in non-treated, adaGb$_3$-treated, or OHEtadaGb$_3$-treated Vero cells. VT2 was bound and internalized at 37 °C for 6 h. VT2 (*green*) and calnexin (*red*) were detected as described for *D*. Fluorescently stained cells were viewed with a confocal microscope. *Arrowhead*, vacuoles; *bar*, 10 μm. Toxin colocalization with organelle markers was quantitated (supplemental Table 2).

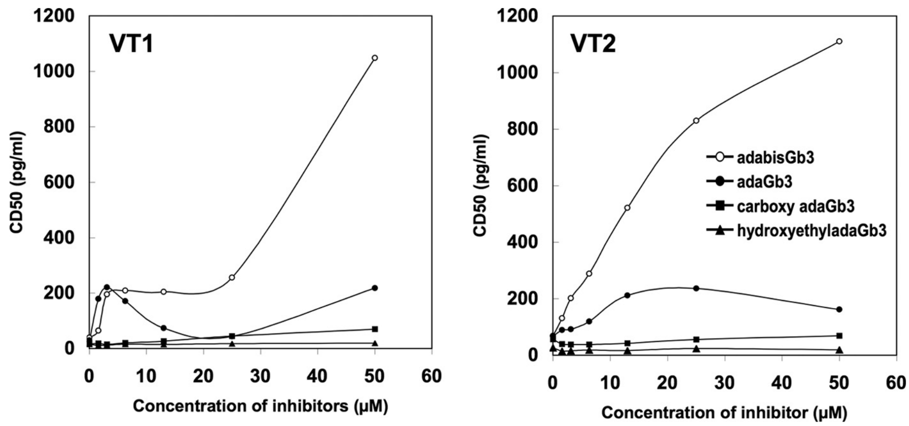

FIGURE 7. **Inhibition of verotoxin cytotoxicity.** Increasing concentrations of adaGb$_3$, carboxyadaGb$_3$, OHEtadaGb$_3$, or adabisGb$_3$ were premixed with VT1 or VT2 dilutions at 37 °C for 1 h and then added to Vero cells for 1 h. Cells were then washed and incubated at 37 °C for 72 h. Live cells were stained with crystal violet, and viability was plotted as a percentage of untreated Vero cells. From this, the CD$_{50}$ values of VT1 (*left*)/VT2 (*right*) preincubated with adaGb$_3$ analogues were determined and plotted as a function of analog concentration.

AdaGb$_3$ Analog Inhibition of VT Cytotoxicity—Previously, we reported that adaGb$_3$ competed with Gb$_3$ for VT1 binding in receptor ELISA (44) and was effective to prevent the Vero cell binding of both VT1 and VT2 (12, 46). We therefore compared the efficacy of other adaGb$_3$ analogues for protection of Vero cells from VT binding.

Increasing concentrations of adaGb$_3$, hydroxylethyladaGb$_3$, carboxyadaGb$_3$, or adabisGb$_3$ were preincubated with VT1/VT2 and tested for reduction of Vero cell cytotoxicity (Fig. 7). Of the "monomer" species, only adaGb$_3$ showed significant protection against VT1 and, more effectively, VT2. CarboxyadaGb$_3$ and hydroxylethyladaGb$_3$ showed no protection. AdabisGb$_3$ inhibited VT1/VT2 Vero cell cytotoxicity to a greater extent than adaGb$_3$. Cytotoxicity of VT1/VT2 preincubated with 50 μM adalbisGb$_3$ was reduced 150–250-fold. AdaGb$_3$ had no effect on Vero cell susceptibility to ricin, which also undergoes Golgi/ER retrograde transport (52); thus, overall transport to the Golgi and ER was not blocked (supplemental Fig. 4).

Unlike Sphingolipids, AdaGb$_3$ Does Not Stabilize Membrane Cholesterol in Phospholipid Liposomes—Because cholesterol is central to intracellular membrane GSL traffic, the ability of Gb$_3$ and adaGb$_3$ to interact with cholesterol was compared by their ability to induce resistance to MβCD cholesterol extraction from a model phospholipid membrane (48, 53). Approximately 40% of the [^{3}H]cholesterol in PC liposomes was extracted by 0.25 mM MβCD (Fig. 8) from the liposomal pellet. Inclusion of SPM or Gb$_3$ within the liposomes significantly reduced the extracted cholesterol to 10 and 15%, respectively, indicating stabilization of the cholesterol within the membrane. In contrast, inclusion of adaGb$_3$ consistently increased cholesterol susceptibility to MβCD extraction to 50%. Inclusion of adaGb$_3$ together with SPM had no effect on SPM-cholesterol stabilization, but adaGb$_3$ reduced the stabilizing effect of Gb$_3$ on cholesterol by ~30%, indicating that membrane adaGb$_3$ interfered with the interaction between Gb$_3$ and cholesterol. Thus, in contrast to Gb$_3$ and SPM, adaGb$_3$ destabilizes rather than stabilizes membrane cholesterol and partially reverses Gb$_3$-cholesterol stabilization. This effect could explain the lack of adaGb$_3$ Golgi/ER trafficking and the adaGb$_3$ modulation of VT1-bound Gb$_3$ intracellular trafficking observed.

AdaGb$_3$ Does Not Alter Internalization and Retrograde Traffic of CT—To address whether the effect of adaGb$_3$ on native Gb$_3$-mediated VT intracellular traffic might be in any way selective, we examined the intracellular retrograde traffic of GM1-bound Cy3-CTB in adaGb$_3$-treated HEK-293 cells. VT1 and CT preferentially bind different Vero cell subsets during the cell cycle (54), making comparison of differential trafficking in a single cell difficult. CHO cells do not express GM1 (55) (or Gb$_3$), and cell suspension cultures (Jurkat) are inconvenient to study intracellular traffic. We therefore treated HEK-293 cells (Gb$_3$−ve, GM1+ve) with adaGb$_3$ and monitored the cell binding and internalization of VT1B and CTB (Fig. 9). The cell surface binding of CTB to HEK-293 cells at 4 °C was largely unaffected by adaGb$_3$ treatment (Fig. 9). VTB bound the HEK-293 cell surface only after adaGb$_3$ treatment and colocalized extensively with CTB at 4 °C (Fig. 9). Warming to 37 °C induced plasma membrane-bound CTB internalization to the same juxtanuclear Golgi structures in both control and adaGb$_3$-treated cells (Fig. 9). VTB, however, was internalized into punctate intracellular vesicles, for the most part, distinct from CTB-labeled Golgi (Fig. 9). VTB containing vesicles were in the Golgi area (as defined by CTB) but remained separate from CTB. Thus, cell surface-colocalized GM1-bound CTB and adaGb$_3$-bound VTB are differentially trafficked to separate structures within the cell, such that GM1-CTB Golgi retrograde traffic is retained, whereas adaGb$_3$-VT1 is trafficked to an alternative destination within the same cells.

DISCUSSION

The binding of the VT family of AB$_5$ subunit toxins to their receptor GSL, globotriaosyl ceramide, is of interest for many reasons. First, the VT B subunit pentamer binding to Gb$_3$ provides the basis for renal glomerular endothelial cell targeting following systemic verotoxemia and therefore plays a central role in the pathology of HUS (17, 56), which remains a life-threatening complication of gastrointestinal verotoxin-producing *E. coli* infection, an ever increasing threat in the devel-

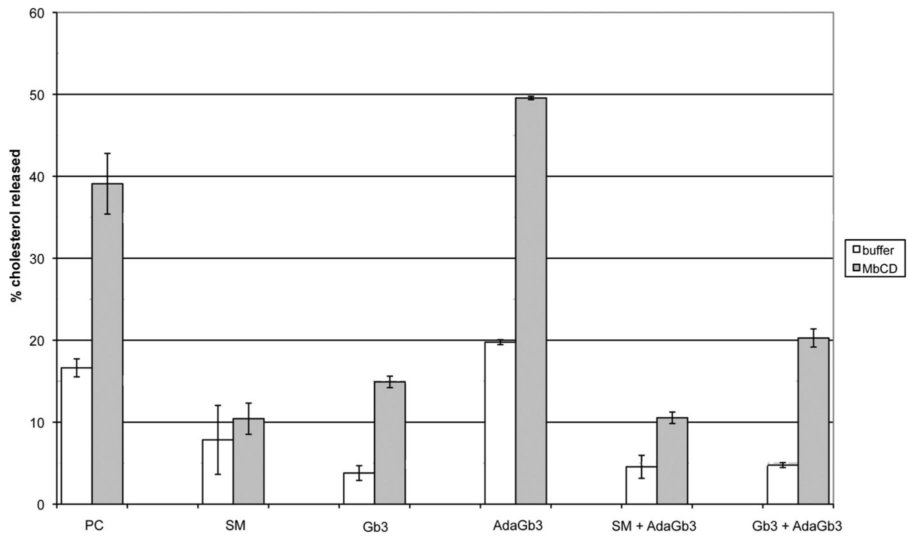

FIGURE 8. **GSLs/adaGSL stabilize/destabilize cholesterol within PC liposomes.** The effect of inclusion of SPM, Gb$_3$, or adaGb$_3$ (alone and in combination) on [^{3}H]cholesterol availability to MβCD extraction from cholesterol/PC liposomes was determined. The percentage of cholesterol extracted by PBS (*open bars*) or 0.25 mM MβCD (*gray bars*) after 1 h at room temperature is shown. As expected, inclusion of the sphingolipid SPM or Gb$_3$ increased resistance to cholesterol extraction by MβCD, but adaGb$_3$ showed a reverse effect. Moreover the inclusion of adaGb$_3$ together with Gb$_3$, but not SPM, partially reversed the stabilizing effect on liposomal cholesterol. *Error bars*, S.D.

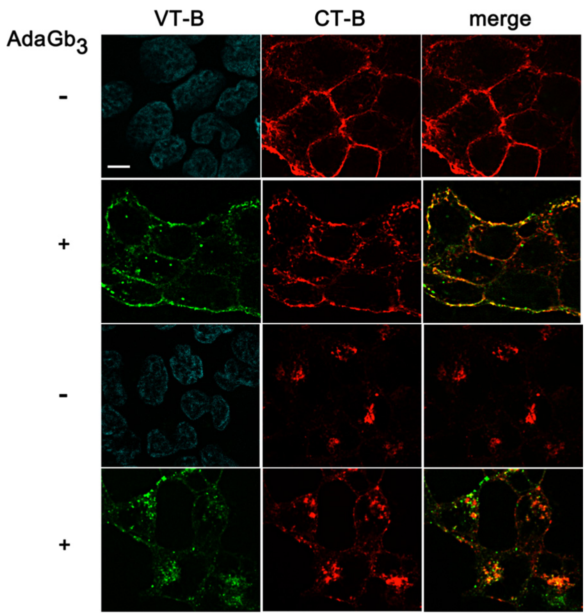

FIGURE 9. **AdaGb$_3$ insertion and VT trafficking do not perturb the intracellular traffic of cholera toxin.** AdaGb$_3$ was inserted into HEK-293 cells, and the simultaneous binding and internalization of Alexa488-VTB and Cy3-CTB were assessed. *Top panels*, binding at 4 °C; *bottom panels*, detection after 1 h of internalization at 37 °C. DAPI nuclear staining is shown for VT1 B-treated cells without adaGb$_3$. *Bar*, 10 μm. Only plasma membrane staining is seen at 4 °C. AdaGb$_3$-bound VTB and GM1-bound CTB show significant cell surface overlap. At 37 °C, Cy3-CTB is internalized to juxtanuclear Golgi in both control and adaGb$_3$-treated cells. In contrast, Alexa488-VTB is internalized to punctate vesicles distinct from CTB-labeled Golgi in adaGb$_3$-treated cells.

oped world (9). Second, verotoxin binding to cell surface Gb$_3$ provides an index of the complex manner in which cell surface GSLs can be presented within a bilayer for ligand recognition and is thus a probe for GSL membrane organization (57). Third, Gb$_3$ and verotoxin internalization and intracellular traffic provide a probe of the molecular basis of retrograde transport to the ER (58). Fourth, Gb$_3$ is up-regulated in many human tumor cells, and thus verotoxin itself (59, 60, 61) or the B subunit pentamer coupled to cytotoxic drugs (62, 63) offers new antineoplastic approaches (64). In this area also, as with HUS, endothelial cells within the neovasculature express Gb$_3$ and are VT-sensitive (65, 66). Last, Gb$_3$ expression is a key risk factor for HIV susceptibility (67), and aglycone modulation of gp120-Gb$_3$ binding is similar to that of VT1 (16).

Membrane GSL organization and its role in intracellular vesicular traffic are poorly understood but are of high potential significance (68–70). The amphipathic GSL analogues we have made, which in part retain the receptor function of membrane GSLs (71), provide new insight into these processes and the means to alter cellular GSL metabolism selectively (72). We now show that adaGSLs have an immediate effect on plasma membrane GSL receptor function and intracellular traffic. Our results, summarized in Scheme 1, include several novel observations as described below.

Induction of VT1/VT2 Cell Sensitivity—We synthesized a series of modified adaGb$_3$ species and found preferential VT2 (*cf.* VT1) binding. These Gb$_3$ mimics incorporated into the plasma membrane of receptor negative cells to induce cell VT1/VT2 cytotoxicity. This is the first report in which a Gb$_3$ derivative has been shown capable of this function and opens the potential to make any cell sensitive to VT cytopathology. Significantly, in such "pseudoreceptor"-reconstituted cells, the toxin-receptor complex was internalized to endosomes but did not mediate Golgi/ER retrograde transport, as for endogenous Gb$_3$-mediated VT traffic (Scheme 1). Despite the different functional groups present, this was seen for all adaGb$_3$ species. Prolonged association with EEA1 vesicles was seen for OHEtadaGb$_3$ but not other adaGb$_3$-treated cells. Lack of Golgi/ER targeting suggests that A-subunit cytosolic translocation from endosomes mediates the induced toxicity (51, 73). The internalized toxin was less long-lived compared with that within Vero cells. (70–100% *versus* 30–50% loss in 1–6 h; see supplemental Table 2). This may indicate proteolysis or, more likely, loss due to recycling from endosomes to the cell surface

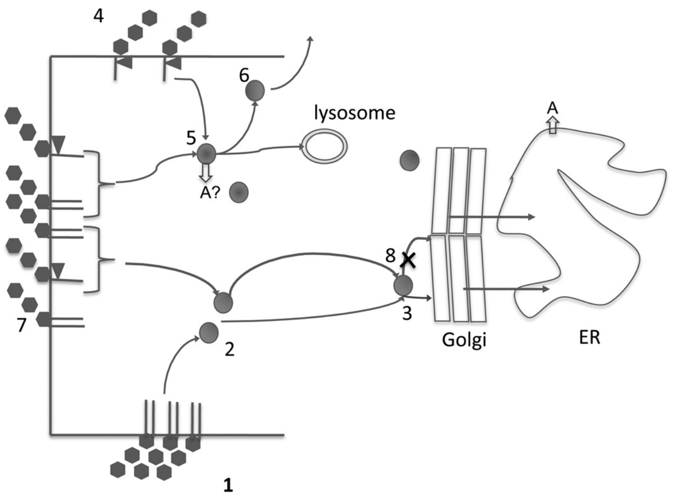

SCHEME 1. *1–3*, endogenous Gb$_3$ within cell surface lipid rafts mediates VT internalization (*1*), endosomal transport to Golgi-associated vesicle (*2*), and retrograde transport to Golgi and thence ER (*3*). *4*, plasma membrane adaGb$_3$ can mediate VT internalization to early endosomes without further retrograde transport. *5*, A-subunit may be released into cytosol. *6*, toxin-adaGb$_3$ complex may be recycled and lost from the cell surface. Some VT may undergo lysosomal degradation. *7*, mixing of endogenous and adaGb$_3$ alters Gb$_3$ organization to disburse Gb$_3$ from raft restriction. In combination, Gb$_3$ and adaGb$_3$ mediate VT internalization to endosomes (*5*) or Golgi-associated vesicles (*3*), but retrograde transport (*8*) to Golgi and ER does not occur.

(Scheme 1). This VT loss from endosomes may contribute to the lack of Golgi/ER VT detection. We have not observed any adaGSL breakdown within the time frame of the present experiments.

The intracellular transport of adaGb$_3$ is distinct from exogenous BODIPY and NBD-GSL analogues, which readily traffic from the cell surface to the Golgi (31). The more planar structure of these fluorescent substituents may permit a cholesterol interaction. This clearly shows that the lipid structure of membrane GSLs can provide differential intracellular membrane addresses for exogenous (and, by inference, endogenous) GSL species. AdaGSLs may be defective in lateral membrane "connectivity" (74).

AdaGb$_3$-reconstituted CHO cells were significantly less sensitive to VT1/VT2 than similarly reconstituted Jurkat cells. This indicates that properties in addition to receptor status regulate cytotoxicity.

AdabisGb$_3$ Does Not Induce VT1/VT2 Cell Sensitivity—Our second novel observation is that adabisGb$_3$, in which two lyso-Gb$_3$s are coupled to a single adamantane frame, does not incorporate into the cell membrane. This lack of membrane partitioning of adabisGb$_3$ is of significance and must be a structure-related property. Although the hydrophobicity of adabisGb$_3$ is significantly reduced compared with adaGb$_3$, gangliosides of greater polarity are readily taken up into the membranes of cultured cells (75). It is possible that the 1–3 coupling to the adamantane frame positions the sphingosine tails in a skewed orientation relative to one another, and as such, the non-parallel alkyl chains may be unable to insert and stack in a lamellar bilayer to prevent plasma membrane incorporation. Nevertheless, in solution, adabisGb$_3$ can bind to VT1/VT2 tightly to function as an extracellular inhibitor of VT1/VT2 cell binding. Furthermore, adabisGb$_3$ itself is not toxic to Jurkat cells, whereas high concentrations of adaGb$_3$ can be toxic. This is probably a function of the lack of cell membrane insertion of adabisGb$_3$. Thus, adabisGb$_3$ provides a potential basis for protection against verotoxemia.

AdaGb$_3$ Compromises Endogenous Gb$_3$-mediated VT1 Retrograde Transport—Our third observation is that adaGb$_3$ can subvert the natural retrograde transport of VT1/VT2 bound to endogenous cellular Gb$_3$. This property is dependent on the lipid structure of the Gb$_3$ mimic; OHEtadaGb$_3$ did not have this effect. In addition, the effect was selective, in that GM1-CTB intracellular traffic was virtually unaffected. AdaGb$_3$ plasma membrane incorporation altered the surface distribution of VT1 and VT2 overall, generating a more uniform cell surface receptor (Gb$_3$ + adaGb$_3$) distribution. This implies cooperation between the membrane-incorporated adaGb$_3$ and non-uniformly distributed Gb$_3$ (Scheme 1). The subsequent retrograde transport of VT1/VT2 from endosomes to Golgi and hence to ER was largely circumvented in adaGb$_3$-treated Vero cells. Consistent with the lack of retrograde Golgi/ER transport, VT1/VT2 cytotoxicity for adaGb$_3$-treated cells became insensitive to BFA protection. VT1 (but not VT2) cytotoxicity was significantly reduced for adaGb$_3$-treated Vero cells, suggesting more effective cytosolic VT2 A-subunit translocation from endosomes.

Lipid Structural Dependence—The early intracellular transport of VT-bound adaGb$_3$ in Gb$_3$-negative cells is similar to endogenous Gb$_3$-bound VT, in that the toxin is rapidly targeted to early endosomes. We did not observe any VT/adaGb$_3$ colocalization with Lamp-2, indicating a fate other than lysosomal degradation. For Gb$_3$-positive plasma membranes into which adaGb$_3$ is incorporated, VT1 and VT2 must simultaneously bind both endogenous Gb$_3$ and incorporated adaGb$_3$. The VTB subunit pentamer will probably bind five Gb$_3$ molecules (76) to induce membrane curvature by compaction (77). Membrane adaGb$_3$ has a larger molecular area and is more resistant to compression than Gb$_3$ (25), and inclusion within this toxin-GSL membrane complex could compromise compaction/membrane curvature. The non-uniform Vero cell distribution of Gb$_3$, as detected by VT1 or VT2 binding, was rendered more uniform after adaGb$_3$ incorporation, consistent with a lack of clustering (77). This redistribution was not seen after OHEtadaGb$_3$ incorporation and correlates with protection against VT cytotoxicity by adaGb$_3$ but not OHEtadaGb$_3$.

Subsequent internalization was similar for adaGb$_3$-treated CHO or Jurkat cells and, initially, for untreated Vero cells, in that early endosomes were targeted, but in adaGb$_3$-treated cells, the later retrograde transport to Golgi/ER was compromised. Thus, the adaGb$_3$ internalization and trafficking route dominated that of endogenous Gb$_3$. This was not observed for OHEtadaGb$_3$-treated cells.

Retrograde transport overall was not affected because Vero cell susceptibility to ricin and Golgi traffic of cholera toxin/GM1 in HEK-293 cells were unaffected by adaGb$_3$. Our previous studies showed partial cell surface colocalization but the separate internalization of VT1 and CT (78). Internalization is mediated through both clathrin-dependent and clathrin-independent mechanisms, both of which access Golgi/ER retrograde transport (27). Although VT2 bound adaGb$_3$ in preference to native Gb$_3$ by TLC overlay, adaGb$_3$ did not have a greater effect on VT2 compared with VT1 intracellular traffic, indicating that membrane organization rather than binding *per se* is the key factor.

AdaGb$_3$ Does Not Interact with Cholesterol—The endosome to TGN transport of VT is compromised by clathrin blockade (79, 80). Cholesterol depletion can reduce both clathrin-dependent (81) and caveolin-dependent (82) internalization and can block actin-dependent endosome-TGN CT (83) and endosome-TGN ricin retrograde transit (84). GSL-cholesterol interaction is key to the formation of liquid-ordered domains in model membranes (85) and increased order in cell membranes (74). Aberrant cholesterol and GSL retrograde transport (and metabolism) are intimately connected in sphingolipid storage diseases (86).

AdaGb$_3$ was unable to stabilize liposomal membrane cholesterol and partially reduced cholesterol stabilization by Gb$_3$; these novel biophysical properties may explain the effect of adaGb$_3$ on intracellular VT routing. If the transition of VT1/VT2-bound Gb$_3$ between endosomes and TGN is cholesterol-dependent, adaGb$_3$-bound VT should transit ineffectively. Similarly, if the punctate cell surface Gb$_3$ distribution were cholesterol-dependent, a more uniform distribution for adaGb$_3$ would be expected.

In adaGb$_3$-treated cells, VT1/VT2 cell surface distribution was altered, but internalization was similar. Thus, the cholesterol-dependent "decision" to undergo Golgi/ER retrograde transport may be taken at the cell surface.

GSL-cholesterol interaction can promote (25) or prevent ligand-GSL binding (21). This may be a function of GSL fatty acid content (16, 20), GSL/cholesterol ratio (20), and membrane curvature (21). The carbohydrate conformation of GSLs is changed when in complex with cholesterol (20). Hydrogen bonding of the sterol OH and adjacent GSL anomeric oxygen "bends" the carbohydrate from a membrane perpendicular to parallel orientation (18, 20, 87), restricts exogenous ligand binding (21), and shields the sterol from water interaction by an "umbrella" effect (87). In model membranes, the GSL glycan thickness is an inverse function of the cholesterol concentration, from perpendicular (thickest) to parallel (thinnest) (20), suggesting a range of intermediate cholesterol-dependent carbohydrate conformations. Nine potential membrane GSL carbohydrate conformations have been modeled (88).

The lack of cholesterol interaction we show predicts ada-GSLs to be resistant to this masking effect, and such analogues might therefore have a binding advantage over natural GSL species in cholesterol-containing membranes. This could explain the dominant trafficking effect of adaGb$_3$ in Gb$_3$-expressing cells and the ability of adamantyl monohexosyl ceramides to modulate GSL metabolism (72). The lack of OHEtadaGb$_3$ efficacy could be consistent with this mechanism. The GSL conformational change induced by cholesterol is mimicked in GSLs containing 2-hydroxy fatty acids (18). Hydrogen bonding between the sugar and fatty acid OH can similarly bend the carbohydrate (89). The OH of OHEtadaGb$_3$ might similarly mediate such a carbohydrate conformational change, and the potential ligand binding advantage would be lost.

OHEtadaGb$_3$ induced VT susceptibility in Gb$_3$-negative cells. In OHEtadaGb$_3$-treated (or carboxyadaGb$_3$- or urea-adaGb$_3$-treated), Gb$_3$-negative cells, intracellular VT trafficking is similar to that of adaGb$_3$-treated cells. This suggested that the incorporated adaGb$_3$ analogues define a shared intracellular retrograde routing, which is different from natural Gb$_3$ traffic. The differential VT cell sensitivity may due to binding differences between adaGb$_3$ analogues. AdaGb$_3$ is strongly bound by VT1/VT2. VT1-adaGb$_3$ binding was similar to VT1-Gb$_3$ binding, and VT2-adaGb$_3$ binding was ~4-fold greater than VT2-Gb$_3$ binding. On the other hand, VT1/OHEtadaGb$_3$ binding was significantly less than VT1/adaGb$_3$ or Gb$_3$. VT2/OHEtadaGb$_3$ binding was similar to VT2/Gb$_3$ binding, significantly weaker than VT2/adaGb$_3$ binding. These binding differences are consistent with an OHEtadaGb$_3$ conformational restriction that could explain the VT sensitivity, cell surface staining, and intracellular trafficking observed in adaGb$_3$-treated *versus* OHEtadaGb$_3$-treated Vero cells. The punctate VT1/VT2 Vero cell surface staining of Gb$_3$-containing plasma membrane domains that we observed at 4 °C, as previously (12), was replaced in adaGb$_3$-treated Vero cells by a more uniform membrane staining pattern. Membrane-incorporated adaGb$_3$ may intercalate to disperse such domains by reducing cholesterol interaction and "fill the gaps" between domains (Scheme 1). This may reroute intracellular traffic similar to non-raft, as compared with raft Gb$_3$ (22).

We found that the VT2-induced vacuolation we previously reported for a subpopulation of Vero cells (12) was retained for adaGb$_3$-treated or OHEtadaGb$_3$-treated Vero cells. Thus, this vacuolation response is independent of VT2 retrograde traffic to the Golgi/ER, which may relate to the increased clinical severity of VT2. In Vero cells, VT2 was present in the limiting membrane of the VT2-induced vacuoles. However, for adaGb$_3$-treated or OHEtadaGb$_3$-treated Vero cells, VT2 was not detected in the vacuolar membrane, indicating that the vacuoles arise from a signaling mechanism rather than direct effect of toxin membrane Gb$_3$ binding.

In conclusion, we show the novel, lipid-dependent, pseudoreceptor function of adaGb$_3$ mimics in receptor negative cells and their structure-dependent domination over native intracellular Gb$_3$-dependent but not GM1-dependent traffic. This may be mediated by the lack of cholesterol association of adaGb3 mimics and their ability to preferentially reduce membrane Gb$_3$-cholesterol interaction.

REFERENCES

1. Spitalnik, P. F., and Spitalnik, S. L. (1995) The P blood group system. Biochemical, serological, and clinical aspects. *Transfus. Med. Rev.* **9,** 110–122
2. Mangeney, M., Richard, Y., Coulaud, D., Tursz, T., and Wiels, J. (1991) CD77. An antigen of germinal center B cells entering apoptosis. *Eur. J. Immunol.* **21,** 1131–1140
3. O'Brien, A. D., Tesh, V. L., Donohue-Rolfe, A., Jackson, M. P., Olsnes, S., Sandvig, K., Lindberg, A. A., and Keusch, G. T. (1992) Shiga toxin. Biochemistry, genetics, mode of action, and role in pathogenesis. *Curr. Top. Microbiol. Immunol.* **180,** 65–94
4. Karmali, M. A., Gannon, V., and Sargeant, J. M. (2010) Verocytotoxin-producing *Escherichia coli* (VTEC). *Vet. Microbiol.* **140,** 360–370
5. Richardson, S. E., Karmali, M. A., Becker, L. E., and Smith, C. R. (1988) The histopathology of the hemolytic uremic syndrome associated with verocytotoxin-producing *Escherichia coli* infections. *Hum. Pathol.* **19,** 1102–1108

6. Müthing, J., Schweppe, C. H., Karch, H., and Friedrich, A. W. (2009) Shiga toxins, glycosphingolipid diversity, and endothelial cell injury. *Thromb. Haemost.* **101,** 252–264
7. Goldwater, P. N. (2007) Treatment and prevention of enterohemorrhagic *Escherichia coli* infection and hemolytic uremic syndrome. *Expert Rev. Anti Infect. Ther.* **5,** 653–663
8. Bielaszewska, M., Mellmann, A., Zhang, W., Köck, R., Fruth, A., Bauwens, A., Peters, G., and Karch, H. (2011) Characterization of the *Escherichia coli* strain associated with an outbreak of haemolytic uraemic syndrome in Germany, 2011. A microbiological study. *Lancet Infect. Dis.* **11,** 671–676
9. Frank, C., Werber, D., Cramer, J. P., Askar, M., Faber, M., an der Heiden, M., Bernard, H., Fruth, A., Prager, R., Spode, A., Wadl, M., Zoufaly, A., Jordan, S., Kemper, M. J., Follin, P., Müller, L., King, L. A., Rosner, B., Buchholz, U., Stark, K., Krause, G., and HUS Investigation Team (2011) Epidemic profile of Shiga toxin-producing *Escherichia coli* O104:H4 outbreak in Germany. *N. Engl. J. Med.* **365,** 1771–1780
10. Karch, H., Friedrich, A. W., Gerber, A., Zimmerhackl, L. B., Schmidt, M. A., and Bielaszewska, M. (2006) New aspects in the pathogenesis of enteropathic hemolytic uremic syndrome. *Semin. Thromb. Hemost.* **32,** 105–112
11. Kawano, K., Okada, M., Haga, T., Maeda, K., and Goto, Y. (2008) Relationship between pathogenicity for humans and stx genotype in Shiga toxin-producing Escherichia coli serotype O157. *Eur. J. Clin. Microbiol. Infect. Dis.* **27,** 227–232
12. Tam, P., Mahfoud, R., Nutikka, A., Khine, A. A., Binnington, B., Paroutis, P., and Lingwood, C. (2008) Differential intracellular transport and binding of verotoxin 1 and verotoxin 2 to globotriaosylceramide-containing lipid assemblies. *J. Cell. Physiol.* **216,** 750–763
13. Okuda, T., Tokuda, N., Numata, S., Ito, M., Ohta, M., Kawamura, K., Wiels, J., Urano, T., Tajima, O., and Furukawa, K. (2006) Targeted disruption of Gb3/CD77 synthase gene resulted in the complete deletion of globo-series glycosphingolipids and loss of sensitivity to verotoxins. *J. Biol. Chem.* **281,** 10230–10235
14. Nyholm, P. G., Magnusson, G., Zheng, Z., Norel, R., Binnington-Boyd, B., and Lingwood, C. A. (1996) Two distinct binding sites for globotriaosyl ceramide on verotoxins. Identification by molecular modeling and confirmation using deoxy analogues and a new glycolipid receptor for all verotoxins. *Chem. Biol.* **3,** 263–275
15. Chark, D., Nutikka, A., Trusevych, N., Kuzmina, J., and Lingwood, C. (2004) Differential carbohydrate epitope recognition of globotriaosyl ceramide by verotoxins and monoclonal antibody: Role in human renal glomerular binding. *Eur. J. Biochem.* **271,** 405–417
16. Mahfoud, R., Manis, A., and Lingwood, C. (2009) Fatty acid-dependent globotriaosyl ceramide receptor function in detergent-resistant model membranes. *J. Lipid Res.* **50,** 1744–1755
17. Khan, F., Proulx, F., and Lingwood, C. A. (2009) Detergent-resistant globotriaosyl ceramide may define verotoxin/glomeruli-restricted hemolytic uremic syndrome pathology. *Kidney Int.* **75,** 1209–1216
18. Yahi, N., Aulas, A., and Fantini, J. (2010) How cholesterol constrains glycolipid conformation for optimal recognition of Alzheimer's β amyloid peptide (Aβ1–40). *PLoS One* **5,** e9079
19. Kaiser, H. J., Lingwood, D., Levental, I., Sampaio, J. L., Kalvodova, L., Rajendran, L., and Simons, K. (2009) Order of lipid phases in model and plasma membranes. *Proc. Natl. Acad. Sci. U.S.A.* **106,** 16645–16650
20. Lingwood, D., Binnington, B., Róg, T., Vattulainen, I., Grzybek, M., Coskun, U., Lingwood, C. A., and Simons, K. (2011) Cholesterol modulates glycolipid conformation and receptor activity. *Nat. Chem. Biol.* **7,** 260–262
21. Mahfoud, R., Manis, A., Binnington, B., Ackerley, C., and Lingwood, C. A. (2010) A major fraction of glycosphingolipids in model and cellular cholesterol-containing membranes is undetectable by their binding proteins. *J. Biol. Chem.* **285,** 36049–36059
22. Falguières, T., Mallard, F., Baron, C., Hanau, D., Lingwood, C., Goud, B., Salamero, J., and Johannes, L. (2001) Targeting of Shiga toxin B-subunit to retrograde transport route in association with detergent-resistant membranes. *Mol. Biol. Cell* **12,** 2453–2468
23. Smith, D. C., Sillence, D. J., Falguières, T., Jarvis, R. M., Johannes, L., Lord, J. M., Platt, F. M., and Roberts, L. M. (2006) The association of Shiga-like toxin with detergent-resistant membranes is modulated by glucosylceramide and is an essential requirement in the endoplasmic reticulum for a cytotoxic effect. *Mol. Biol. Cell* **17,** 1375–1387
24. Hooper, N. (1999) Detergent-insoluble glycosphingolipid/cholesterol-rich membrane domains, lipid rafts and caveolae (review). *Mol. Membr. Biol.* **16,** 145–156
25. Mahfoud, R., Mylvaganam, M., Lingwood, C. A., and Fantini, J. (2002) A novel soluble analog of the HIV-1 fusion cofactor, globotriaosylceramide (Gb$_3$), eliminates the cholesterol requirement for high affinity gp120/Gb$_3$ interaction. *J. Lipid Res.* **43,** 1670–1679
26. Sandvig, K., Olsnes, S., Brown, J. E., Petersen, O. W., and van Deurs, B. (1989) Endocytosis from coated pits of Shiga toxin. A glycolipid-binding protein from *Shigella dysenteriae* 1. *J. Cell Biol.* **108,** 1331–1343
27. Nichols, B. J., Kenworthy, A. K., Polishchuk, R. S., Lodge, R., Roberts, T. H., Hirschberg, K., Phair, R. D., and Lippincott-Schwartz, J. (2001) Rapid cycling of lipid raft markers between the cell surface and Golgi complex. *J. Cell Biol.* **153,** 529–541
28. Sandvig, K., Garred, O., Prydz, K., Kozlov, J. V., Hansen, S. H., and van Deurs, B. (1992) Retrograde transport of endocytosed Shiga toxin to the endoplasmic reticulum. *Nature* **358,** 510–512
29. Tam, P. J., and Lingwood, C. A. (2007) Membrane cytosolic translocation of verotoxin A1 subunit in target cells. *Microbiology* **153,** 2700–2710
30. Hoey, D. E., Sharp, L., Currie, C., Lingwood, C. A., Gally, D. L., and Smith, D. G. (2003) Verotoxin 1 binding to intestinal crypt epithelial cells results in localization to lysosomes and abrogation of toxicity. *Cell. Microbiol.* **5,** 85–97
31. Pagano, R. E., Puri, V., Dominguez, M., and Marks, D. L. (2000) Membrane traffic in sphingolipid storage diseases. *Traffic* **1,** 807–815
32. Johannes, L., Pezo, V., Mallard, F., Tenza, D., Wiltz, A., Saint-Pol, A., Helft, J., Antony, C., and Benaroch, P. (2003) Effects of HIV-1 Nef on retrograde transport from the plasma membrane to the endoplasmic reticulum. *Traffic* **4,** 323–332
33. Kiarash, A., Boyd, B., and Lingwood, C. A. (1994) Glycosphingolipid receptor function is modified by fatty acid content. Verotoxin 1 and verotoxin 2c preferentially recognize different globotriaosyl ceramide fatty acid homologues. *J. Biol. Chem.* **269,** 11138–11146
34. Boyd, B., Magnusson, G., Zhiuyan, Z., and Lingwood, C. A. (1994) Lipid modulation of glycolipid receptor function. Availability of Gal(α1–4)Gal disaccharide for verotoxin binding in natural and synthetic glycolipids. *Eur. J. Biochem.* **223,** 873–878
35. Arab, S., and Lingwood, C. A. (1996) Influence of phospholipid chain length on verotoxin/globotriaosyl ceramide binding in model membranes. Comparison of a supported bilayer film and liposomes. *Glycoconj. J.* **13,** 159–166
36. Lingwood, C. A. (1996) Aglycone modulation of glycolipid receptor function. *Glycoconj. J.* **13,** 495–503
37. Sandvig, K., and van Deurs, B. (2002) Transport of protein toxins into cells. Pathways used by ricin, cholera toxin, and Shiga toxin. *FEBS Lett.* **529,** 49–53
38. Lencer, W. I., and Tsai, B. (2003) The intracellular voyage of cholera toxin. Going retro. *Trends Biochem. Sci.* **28,** 639–645
39. Pagano, R. E., Watanabe, R., Wheatley, C., and Dominguez, M. (2000) Applications of BODIPY-sphingolipid analogs to study lipid traffic and metabolism in cells. *Methods Enzymol.* **312,** 523–534
40. Kitov, P. I., Sadowska, J. M., Mulvey, G., Armstrong, G. D., Ling, H., Pannu, N. S., Read, R. J., and Bundle, D. R. (2000) Shiga-like toxins are neutralized by tailored multivalent carbohydrate ligands. *Nature* **403,** 669–672
41. Nishikawa, K., Matsuoka, K., Watanabe, M., Igai, K., Hino, K., Hatano, K., Yamada, A., Abe, N., Terunuma, D., Kuzuhara, H., and Natori, Y. (2005) Identification of the optimal structure required for a Shiga toxin neutralizer with oriented carbohydrates to function in the circulation. *J. Infect. Dis.* **191,** 2097–2105
42. Kitov, P. I., Mulvey, G. L., Griener, T. P., Lipinski, T., Solomon, D., Paszkiewicz, E., Jacobson, J. M., Sadowska, J. M., Suzuki, M., Yamamura, K., Armstrong, G. D., and Bundle, D. R. (2008) *In vivo* supramolecular templating enhances the activity of multivalent ligands. A potential therapeutic against the *Escherichia coli* O157 AB5 toxins. *Proc. Natl. Acad. Sci. U.S.A.* **105,** 16837–16842

43. St Hilaire, P. M., Boyd, M. K., and Toone, E. J. (1994) Interaction of the Shiga-like toxin type 1 B-subunit with its carbohydrate receptor. *Biochemistry* **33,** 14452–14463
44. Mylvaganam, M., and Lingwood, C. (1999) Adamantyl globotriaosyl ceramide. A monovalent soluble mimic which inhibits verotoxin binding to its glycolipid receptor. *Biochem. Biophys. Res. Commun.* **257,** 391–394
45. Mylvaganam, M., and Lingwood, C. A. (2003) A preamble to aglycone reconstruction for membrane-presented glycolipids. in *Carbohydrate-based Drug Discovery* (Wong, C.-H., ed) pp. 761–780, Wiley-VCH Press, Weinheim, Germany
46. Rutjes, N. W., Binnington, B. A., Smith, C. R., Maloney, M. D., and Lingwood, C. A. (2002) Differential tissue targeting and pathogenesis of verotoxins 1 and 2 in the mouse animal model. *Kidney Int.* **62,** 832–845
47. Petric, M., Karmali, M. A., Richardson, S., and Cheung, R. (1987) Purification and biological properties of *Escherichia coli* verocytotoxin *FEMS Microbiol. Lett.* **41,** 63–68
48. Niu, S. L., and Litman, B. J. (2002) Determination of membrane cholesterol partition coefficient using a lipid vesicle-cyclodextrin binary system. Effect of phospholipid acyl chain unsaturation and headgroup composition. *Biophys. J.* **83,** 3408–3415
49. Halling, K. K., Ramstedt, B., Nyström, J. H., Slotte, J. P., and Nyholm, T. K. (2008) Cholesterol interactions with fluid-phase phospholipids. Effect on the lateral organization of the bilayer. *Biophys. J.* **95,** 3861–3871
50. Wolf, A. A., Jobling, M. G., Saslowsky, D. E., Kern, E., Drake, K. R., Kenworthy, A. K., Holmes, R. K., and Lencer, W. I. (2008) Attenuated endocytosis and toxicity of a mutant cholera toxin with decreased ability to cluster ganglioside GM1 molecules. *Infect. Immun.* **76,** 1476–1484
51. Khine, A. A., Tam, P., Nutikka, A., and Lingwood, C. A. (2004) Brefeldin A and filipin distinguish two globotriaosyl ceramide/verotoxin-1 intracellular trafficking pathways involved in Vero cell cytotoxicity. *Glycobiology* **14,** 701–712
52. Sandvig, K., and van Deurs, B. (1994) Endocytosis and intracellular sorting of ricin and Shiga toxin. *FEBS Lett.* **346,** 99–102
53. Veiga, M. P., Arrondo, J. L., Goñi, F. M., Alonso, A., and Marsh, D. (2001) Interaction of cholesterol with sphingomyelin in mixed membranes containing phosphatidylcholine, studied by spin-label ESR and IR spectroscopies. A possible stabilization of gel-phase sphingolipid domains by cholesterol. *Biochemistry* **40,** 2614–2622
54. Majoul, I., Schmidt, T., Pomasanova, M., Boutkevich, E., Kozlov, Y., and Söling, H. D. (2002) Differential expression of receptors for Shiga and cholera toxin is regulated by the cell cycle. *J. Cell Sci.* **115,** 817–826
55. Rosales Fritz, V. M., Daniotti, J. L., and Maccioni, H. J. (1997) Chinese hamster ovary cells lacking GM1 and GD1a synthesize gangliosides upon transfection with human GM2 synthase. *Biochim. Biophys. Acta* **1354,** 153–158
56. Lingwood, C. A., Binnington, B., Manis, A., and Branch, D. R. (2010) Globotriaosyl ceramide receptor function. Where membrane structure and pathology intersect. *FEBS Lett.* **584,** 1879–1886
57. Lingwood, C. A., Manis, A., Mahfoud, R., Khan, F., Binnington, B., and Mylvaganam, M. (2010) New aspects of the regulation of glycosphingolipid receptor function. *Chem. Phys. Lipids* **163,** 27–35
58. Sandvig, K., Bergan, J., Dyve, A. B., Skotland, T., and Torgersen, M. L. (2009) Endocytosis and retrograde transport of Shiga toxin. *Toxicon* **56,** 1181–1185
59. Arab, S., Rutka, J., and Lingwood, C. (1999) Verotoxin induces apoptosis and the complete, rapid, long-term elimination of human astrocytoma xenografts in nude mice. *Oncol. Res.* **11,** 33–39
60. Salhia, B., Rutka, J. T., Lingwood, C., Nutikka, A., and Van Furth, W. R. (2002) The treatment of malignant meningioma with verotoxin. *Neoplasia* **4,** 304–311
61. LaCasse, E. C., Bray, M. R., Patterson, B., Lim, W. M., Perampalam, S., Radvanyi, L. G., Keating, A., Stewart, A. K., Buckstein, R., Sandhu, J. S., Miller, N., Banderjee, D., Singh, D., Belch, A. R., Pilarski, L. M., and Gariépy, J. (1999) Shiga-like toxin I receptor on human breast cancer, lymphoma, and myeloma and absence from $CD34^+$ hematopoietic stem cells: Implications for *ex vivo* tumor purging and autologous stem cell transplantation. *Blood* **94,** 2901–2910
62. Falguières, T., Maak, M., von Weyhern, C., Sarr, M., Sastre, X., Poupon, M. F., Robine, S., Johannes, L., and Janssen, K. P. (2008) Human colorectal tumors and metastases express Gb3 and can be targeted by an intestinal pathogen-based delivery tool. *Mol. Cancer Ther.* **7,** 2498–2508
63. Amessou, M., Carrez, D., Patin, D., Sarr, M., Grierson, D. S., Croisy, A., Tedesco, A. C., Maillard, P., and Johannes, L. (2008) Retrograde delivery of photosensitizer (TPPp-*O*-β-GluOH)$_3$ selectively potentiates its photodynamic activity. *Bioconjug. Chem.* **19,** 532–538
64. Đevenica, D., Čikeš Čulić, V., Vuica, A., and Markotić, A. (2011) Biochemical, pathological and oncological relevance of Gb3Cer receptor. *Med. Oncol.* **28,** S675–S684
65. Heath-Engel, H. M., and Lingwood, C. A. (2003) Verotoxin sensitivity of ECV304 cells in vitro and *in vivo* in a xenograft tumor model. VT1 as a tumor neovascular marker. *Angiogenesis* **6,** 129–141
66. Johansson, D., Kosovac, E., Moharer, J., Ljuslinder, I., Brännström, T., Johansson, A., and Behnam-Motlagh, P. (2009) Expression of verotoxin-1 receptor Gb3 in breast cancer tissue and verotoxin-1 signal transduction to apoptosis. *BMC Cancer* **9,** 67
67. Lund, N., Olsson, M. L., Ramkumar, S., Sakac, D., Yahalom, V., Levene, C., Hellberg, A., Ma, X. Z., Binnington, B., Jung, D., Lingwood, C. A., and Branch, D. R. (2009) The human p^k histo-blood group antigen provides protection against HIV-1 infection. *Blood* **113,** 4980–4991
68. Sillence, D. J., Puri, V., Marks, D. L., Butters, T. D., Dwek, R. A., Pagano, R. E., and Platt, F. M. (2002) Glucosylceramide modulates membrane traffic along the endocytic pathway. *J. Lipid Res.* **43,** 1837–1845
69. Patterson, G. H., Hirschberg, K., Polishchuk, R. S., Gerlich, D., Phair, R. D., and Lippincott-Schwartz, J. (2008) Transport through the Golgi apparatus by rapid partitioning within a two-phase membrane system. *Cell* **133,** 1055–1067
70. Zhang, H., Abraham, N., Khan, L. A., Hall, D. H., Fleming, J. T., and Göbel, V. (2011) Apicobasal domain identities of expanding tubular membranes depend on glycosphingolipid biosynthesis. *Nat. Cell Biol.* **13,** 1189–1201
71. Lingwood, C. A., Sadacharan, S., Abul-Milh, A., Mylvaganam, M., and Peter, M. (2006) Soluble adamantyl glycosphingolipid analogs as probes of glycosphingolipid function. in *Glycobiology Protocols* (Braukhausen, I., ed) pp. 305–320, Humana Press, Totowa, NJ
72. Kamani, M., Mylvaganam, M., Tian, R., Rigat, B., Binnington, B., and Lingwood, C. (2011) Adamantyl glycosphingolipids provide a new approach to the selective regulation of cellular glycosphingolipid metabolism. *J. Biol. Chem.* **286,** 21413–21426
73. McKenzie, J., Johannes, L., Taguchi, T., and Sheff, D. (2009) Passage through the Golgi is necessary for Shiga toxin B subunit to reach the endoplasmic reticulum. *FEBS J.* **276,** 1581–1595
74. Lingwood, D., Ries, J., Schwille, P., and Simons, K. (2008) Plasma membranes are poised for activation of raft phase coalescence at physiological temperature. *Proc. Natl. Acad. Sci. U.S.A.* **105,** 10005–10010
75. Schwarzmann, G. (2001) Uptake and metabolism of exogenous glycosphingolipids by cultured cells. *Semin. Cell Dev. Biol.* **12,** 163–171
76. Soltyk, A. M., MacKenzie, C. R., Wolski, V. M., Hirama, T., Kitov, P. I., Bundle, D. R., and Brunton, J. L. (2002) A mutational analysis of the globotriaosylceramide-binding sites of verotoxin VT1. *J. Biol. Chem.* **277,** 5351–5359
77. Windschiegl, B., Orth, A., Römer, W., Berland, L., Stechmann, B., Bassereau, P., Johannes, L., and Steinem, C. (2009) Lipid reorganization induced by Shiga toxin clustering on planar membranes. *PLoS One* **4,** e6238
78. Schapiro, F. B., Lingwood, C., Furuya, W., and Grinstein, S. (1998) pH-independent retrograde targeting of glycolipids to the Golgi complex. *Am. J. Physiol.* **274,** C319–C332
79. Lauvrak, S. U., Torgersen, M. L., and Sandvig, K. (2004) Efficient endosome-to-Golgi transport of Shiga toxin is dependent on dynamin and clathrin. *J. Cell Sci.* **117,** 2321–2331
80. Saint-Pol, A., Yélamos, B., Amessou, M., Mills, I. G., Dugast, M., Tenza, D., Schu, P., Antony, C., McMahon, H. T., Lamaze, C., and Johannes, L. (2004) Clathrin adaptor epsinR is required for retrograde sorting on early endosomal membranes. *Dev. Cell* **6,** 525–538
81. Rodal, S. K., Skretting, G., Garred, O., van Deurs, B., and Sandvig, K. (1999) Extraction of cholesterol with methyl-β-cyclodextrin perturbs formation of clathrin-coated endocytic vesicles. *Mol. Biol. Cell* **10,** 961–974

82. Le, P. U., and Nabi, I. R. (2003) Distinct caveolae-mediated endocytic pathways target the Golgi apparatus and the endoplasmic reticulum. *J. Cell Sci.* **116,** 1059–1071
83. Badizadegan, K., Wheeler, H. E., Fujinaga, Y., and Lencer, W. I. (2004) Trafficking of cholera toxin-ganglioside GM1 complex into Golgi and induction of toxicity depend on actin cytoskeleton. *Am. J. Physiol. Cell Physiol.* **287,** C1453–C1462
84. Spilsberg, B., Van Meer, G., and Sandvig, K. (2003) Role of lipids in the retrograde pathway of ricin intoxication. *Traffic* **4,** 544–552
85. Bacia, K., Schwille, P., and Kurzchalia, T. (2005) Sterol structure determines the separation of phases and the curvature of the liquid-ordered phase in model membranes. *Proc. Natl. Acad. Sci. U.S.A.* **102,** 3272–3277
86. Puri, V., Watanabe, R., Dominguez, M., Sun, X., Wheatley, C. L., Marks, D. L., and Pagano, R. E. (1999) Cholesterol modulates membrane traffic along the endocytic pathway in sphingolipid-storage diseases. *Nat. Cell Biol.* **1,** 386–388
87. Hall, A., Róg, T., Karttunen, M., and Vattulainen, I. (2010) Role of glycolipids in lipid rafts. A view through atomistic molecular dynamics simulations with galactosylceramide. *J. Phys. Chem. B* **114,** 7797–7807
88. Nyholm, P. G., and Pascher, I. (1993) Orientation of the saccharide chains of glycolipids at the membrane surface. Conformational analysis of the glucose-ceramide and the glucose-glyceride linkages using molecular mechanics (MM3). *Biochemistry* **32,** 1225–1234
89. Calander, N., Karlsson, K. A., Nyholm, P. G., and Pascher, I. (1988) On the dissection of binding epitopes on carbohydrate receptors for microbes using molecular modeling. *Biochimie* **70,** 1673–1682